Emergence of slow timescales in development controlled by a temporal morphogen signal

Daniel-Eugen Tufcea

Master of Science

Department of Physics

McGill University Montreal, Quebec 2014-04-15

A thesis submitted to the Faculty of Graduate Studies and Research in partial fulfilment of the requirements for the degree of Master of Science

©Daniel-Eugen Tufcea, 2014

DEDICATION

This thesis is dedicated to my mother Geta Nedelea Tufcea and my father Daniel Tufcea. Thank you for allowing me to do the mistakes I needed to do so that I could one day claim my successes as my own.

ACKNOWLEDGEMENTS

I would like to thank my supervisor, Prof. Paul François, for the continuous support throughout my M. Sc. and for agreeing to take me on as a student on such short notice. I thank him for his patience, his guidance and understanding.

I thank the François group which provided a stimulating environment and helped peer review my work. Special thanks go to Jean-Benoit Lalanne for the long and insightful conversations that helped shape my ideas and ideals. Your hard working and honest personality were an inspiration.

I gratefully acknowledge the funding agencies Natural Science and Engineering Research Council (NSERC) and Human Frontiers Science Program (HFSP) for their generous support.

ABSTRACT

Classical models of differentiation assume that cell fate is determined by the concentration of a static morphogen gradient. In contrast, we provide a setup for in silico differentiation and patterning of embryos under the action of a temporal morphogen signal. We analyze a simplified model for neural tube patterning and use dynamical system theory to uncover the emergence of a slow timescale due to a saddle-node bifurcation. Using the theory of slow manifolds, we give an analytic solution for the canalization of gene expression in phase space. We generalize the patterning mechanism and find gene networks with higher number of genes that lead to an equal number of domains and show that, locally, they are analogous to the low dimensional case. We analyze the model under stochastic conditions with the Langevin equation and find that predictive power decreases as a function of time for low numbers of molecules. We propose a cell-to-cell interaction to confer robustness and restore predictive power. Parameters are found through in silico evolution and the influence of noise is greatly reduced.

ABRÉGÉ

Les modèles classiques de différenciation supposent que le destin des cellules est déterminé par la concentration d'un gradient de morphogène statique. Nous fournissons un modèle pour la différenciation et la structuration des embryons in silico sous l'influence d'un signal de morphogène temporel. Nous analysons un modèle simplifié pour la formation des motifs dans le tube neural et utilisons la théorie des systèmes dynamiques pour découvrir l'émergence d'une échelle de temps lente due à une bifurcation du type col-noeud. Utilisant la théorie des variétés lentes, nous trouvons une solution analytique pour la canalisation de l'expression des gènes dans l'espace des phases. Nous généralisons le mécanisme pour de plus grands réseaux de gènes tout en montrant que, localement, ils ont les mêmes propriétés. Nous analysons le modèle dans toute sa stochasticité avec l'équation de Langevin et constatons qu'il y a une perte du pouvoir de prédiction en fonction du temps. Nous proposons une intéraction de cellule à cellule qui confère de la robustesse et permet de restaurer le pouvoir de prédiction. Les paramètres sont trouvés par évolution in silico et l'influence du bruit est considérablement réduite.

TABLE OF CONTENTS

DEL	DICATI	ON	ii
ACK	KNOW]	LEDGEMENTS	iii
ABS	TRAC	T	iv
ABF	RÉGÉ		V
LIST	OF T	ABLES	viii
LIST	OF F	IGURES	ix
1	INTR	ODUCTION: PRINCIPLES OF DEVELOPMENT	1
	1.1 1.2 1.3	Probing in the dark	2 3 7
2	MOTI	IVATION	9
	2.1 2.2 2.3	Hox genes	9 11 12
3	Dynar	nical system theory for Gene Regulator Networks	16
	3.1 3.2 3.3 3.4 3.5	Genes Regulatory Networks (GRN)	16 22 25 26 29
4	Result	5S	32
	4.1 4.2 4.3 4.4 4.5 4.6	Setup for embryo Phase space Analytical Solution Higher dimension Bifurcation analysis Stochastic analysis 4.6.1 Cell averaging 4.6.2 In Silico Evolution selects for Eint Gint	33 38 40 44 48 51 53 56

5	ssion	58	
	5.1 5.2 5.3	Emergence of timescales and evolvability	59
A	Comp	utational Evolution	63
	A.1 A.2	Evolution Algorithm	
В	Evolu	tion of temporal networks	67
Refe	erences		70

LIST OF TABLES

<u>Table</u>		page
3-1	Example table for the 3D GRN of Fig. 3–2	. 21
4-1	Table for the simplified 2-dimensional GRN of Fig. 4–1	. 33
4-2	Table for the $n=5$ dimensional GRN of Fig. 4–15	. 47
B-1	Table for the $n = 5$ dimensional evolved GRN	69

LIST OF FIGURES

<u>Figure</u>		page
1-1	The French Flag Model explains patterning	4
1-2	French Flag Model and cell grafting.	5
1-3	Temporal French Flag Model	6
2-1	Hox Genes in <i>Drosophila</i> and mouse	10
2-2	The polarizing region and the apical ectodermal ridge in the developing limb bud	12
2-3	Schematics of vertebral neural tube patterning	13
2-4	Graph of GRN explaining neural tube patterning	14
2–5	Experimental Data of neural tube patterning with the use of phosphorescent microscopy	15
3-1	Example Hill functions for gene activation and repression	18
3-2	Graph and Output for an example GRN	20
3-3	Phase portrait of the non-linear pendulum	23
3-4	Phase portrait of a biological switch	27
3-5	Bifurcation diagram of a biological switch	28
3-6	Langevin realization for the biological switch.	31
4-1	Simplified GRN for neural tube patterning	32
4-2	Modeling of S as a traveling wave along the embryo	34
4-3	Graph of S as a function of time and the exposure time	35
4-4	Graph of O,N as a function of time for two different exposure times $\theta.$	36
4-5	Patterning process of a 1D embryo subjected to a temporal morphogen gradient	. 37
4-6	Phase portrait of the simplified network 4–1 at $S=0.6$	38
4–7	Phase portrait of the simplified network 4–1 as a function of S and for $S_+=0.710.$	39
4-8	Bifurcation diagram simplified network 4–1 as a function of $S.$	39
4-9	Change of timescale as a function of S through the closeness to the bifurcation.	40

4–10	Linear solution of Eq. 4.3 for various initial conditions	42
4–11	Implicit plot of the Valley for different values of S	43
4–12	Comparison of phase space velocity, the approximate Valley velocity and the eigenvalues as a function of time	44
4–13	Patterning process into five domains for a 1D embryo subjected to a temporal morphogen gradient	45
4-14	Graph of $M(t)$ as a function of time and the exposure time θ	46
4-15	Graph of generalized 5D GRN	47
4-16	Timecourse of the 5D GRN and associated flow	48
4-17	A bifurcation controls the timescale of individual genes	49
4-18	Nullclines of the 5D GRN	50
4–19	Stochastic ensemble average of the oscillating 5D GRN with a fast timescale, $T_{iM}=1.5.\ldots$	52
4-20	Stochastic ensemble average of the oscillating 5D GRN with a slow timescale, $T_{iM}=1.58.\ldots$	53
4-21	Cell-to-cell interaction function	54
4-22	Stochastic ensemble average with cell-to-cell interaction	57
5–1	Temporary gene knock off in the 5D GRN	60
A-1	Mutual Information of various cell arrays	65
A-2	RMS Fitness for the biological switch	66
B–1	Time course and gene expression domains for an evolved GRN	68

Chapter 1 - INTRODUCTION: PRINCIPLES OF DEVELOPMENT

There is evidently a perception of complexity in living organisms, it is one of the reasons why life is a controversial subject to begin with. We invoke physics and chemistry to formulate the principles by which the world abides, but relegate to biology what goes on inside us. Yet, some treat and teach biology as a descriptive science, cataloging the various processes of life rather than exploring how they emerge from their constituents. And while the division between the living and the inanimate is intuitive, it is not well-defined nor necessarily useful from a molecular point of view. We believe that guided by the principles that served physics so well up to now, we can bridge the gap between the living and the inanimate. The application of a physical way of thinking to biological problems has worked for many problems in the past and there is hope to reduce these complex living organisms to systems of working parts that are more informative.

For the purpose of this thesis, we turn our attention to the specific yet vast subfield of developmental biology. The primary question is How does the fertilized egg give rise to a multicellular organism? This question is too broad to digest on its own and the road to an answer will spawn many more questions. We shall therefore further restrict ourselves to embryonic development and more specifically to the modeling of gene networks under the influence of signaling molecules, termed morphogens, as a means for cell differentiation. An exceptional quality of the developing embryo is the similarly across vastly different species. There are relatively few genes that control development and many species look very alike at their phylotypic stages. As such, we do not attempt to study any particular organism, we instead search for a general principle to answer a precise question: How can a gene regulatory network (GRN) be used to differentiate cells based on a temporal variable such as the exposure time to a morphogen?

1.1 Probing in the dark

Biology has for a long time been constrained by our ability to carry experiments. Each breakthrough in the experimentalist's tool set led to a radically new way of thinking about life. With the advent of the microscope, the discovery of the cell [1] led scientists to abandon of the idea of preformation, that embryos are fully formed and grow in size to become adults. Instead, it is now understood that the embryo starts with a tiny single cell which divides into many more. Those cells themselves further divide and differentiate to form the precursor to structures such organs, limbs or the nervous system.

How those cells differentiated was not clear and, at the time, the experiments consisted of removing cells or grafting them near other cells. In this way, Wilhelm Roux [2] was able to show that when destroying one of the two cells of a frog egg after the first cleavage, the resulting embryo was half developed. A similar experiment by Hans Driesch [3] on a sea urchin, however, gave rise to a whole gastrula, albeit smaller in size. This lead to the developmental process known as regulation. Experiments on newt embryo by Hans Spemann and Hilde Mangold led to the discovery that cells influence the development of neighboring cells [4]. By grafting tissue from the dorsal lip of the blastopore to the blastocoel roof, they obtained an embryo with the induced structure of a second independent embryo.

It took a while for genetics to be recognized as an important player in development. Initially seen as a way to transmit hereditary elements from generation to generation, it wasn't until the 1940s when it became clear that genes encode proteins that they became fundamental to development. It had been understood that proteins determine the properties of cells and by controlling which protein is produced, genes could control development. By the 1960s it was understood that genes could produce proteins which would regulate the activity of other genes, effectively leading to the idea of GRNs.

For a long time developmental genes could only be identified through spontaneous mutations. In particular, mutated recessive genes can be found in heterozygous embryos through their effect on the phenotype. Once a trait was attributed to a single gene, it could be mapped to a region of the chromosome through genetic mapping techniques. Relying on spontaneous mutations and on changes in phenotype was, however, very inconvenient. Advances in chemical and X-ray mutagenesis allowed the discovery of many more developmental genes [5] while

the use of immunostaining and fluorescence imaging made possible the measurement of gene activity in specific cells of the embryo.

Most experiments that shaped the current theory had a major drawback. Experiments were built around measurements taken after a certain time, whether by measuring gene concentration or observing a change in phenotype. Having access to gene concentrations after a certain time, but not to a complete and accurate time series, lead to a static view of development with emphasis on concentration as a function of cell position and cell fate as a steady-state decision. The dynamical nature of gene expression was hard to probe and as a result the methods by which cells time events are still not well understood.

1.2 French Flag Model: A temporal approach

An important question in developmental biology is: How do cells acquire positional information? Cells are organized in the embryo according to their position relative to some axes such as the anterior-posterior and the dorsal-ventral axis or according to their proximity to some structures such as the tail bud in the formation of somities or the limb bud for the formation of limbs. However, for cells to know their position along such axes, there must be something to sense which is specific to that position along the axis. If we imagine that cells responds to a molecule, termed morphogen, we can imagine that a gradient along the axis can specify cell fate. Each cell would sense the concentration and different concentration thresholds would lead to different cell fates. This is the essence of the Wolpert's French Flag Model [6,7] depicted in Fig. 1–1.

These morphogens gradients are often termed fields and they can specify multiple cell fates. If the cells are differentiated a morphogen field can still lead to different cell fates even when exposed to similar concentrations. The typical example is that of the French flag and the USA flag, Fig. 1–2. Cells that make up the French flag can differentiate into either blue, white or red cells, according to the concentration of morphogen they sense. On the other hand, cells that make up the USA flag can either become starry or stripped. If we graft cells from the left side of the French flag to the right side, they would become blue, not red, because they are exposed to a low concentration of morphogen. On the other hand, if we

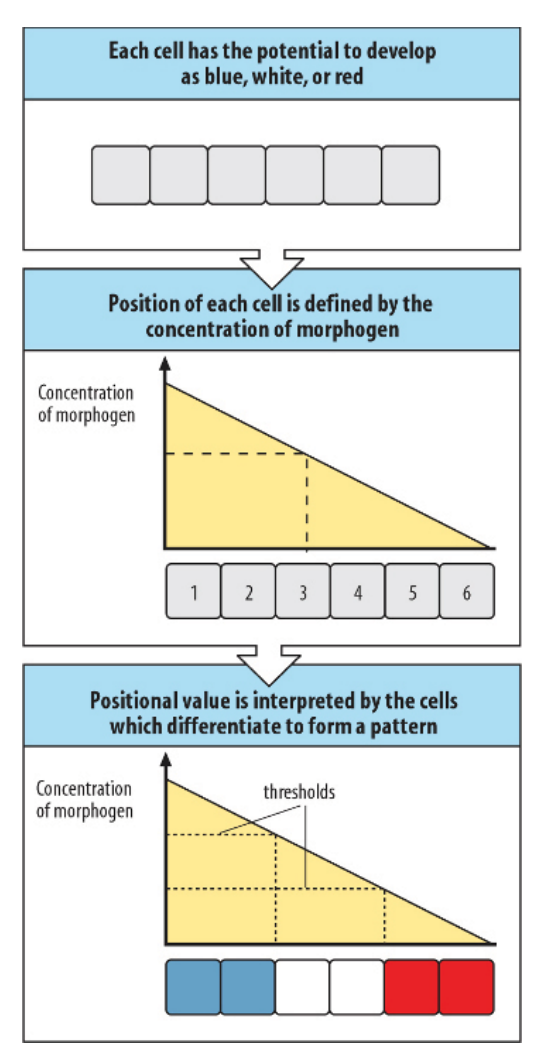


Figure 1–1: The French Flag Model explains how positional information can be interpreted by the cell in order to allow for patterning. Initially, each cell of a given type has the potential to develop as blue, white or red. Each cell has a position along the organism's axis, but cannot on its own determine it. To interpret its positional value, the cell senses the concentration of a morphogen gradient along the axis. Different concentration threshold lead to patterning into blue, white and red cells. As long as the morphogen gradient can be replicated and scaled, the pattern will develop even if half the embryo is removed. Figure reproduced as in *Principles of Development* by Wolpert [6].

grafted cells from the French flag onto the US flag, the grafted cells would keep their French flag identity and differentiate according to their position along the flag's left-right axis.

The French Flag Model is a good example of a regulatory model. Cells do not need to predetermine their fate, it can be given to them as a result of their environment. If we revisit Driesch's experiment on sea urchins, we can explain how the destruction of half the embryo at an early stage can still lead to a fully developed, although smaller embryo. If the morphogen gradient can be re-established, then the entire pattern can be reproduced albeit on a smaller scale. The French Flag Model has also been successful in modeling regeneration, whereby some animals can regenerate missing limbs.

With the advent of real time imaging, movies can now be produced where the expression of genes can be followed as a function of time [8]. This opens up the possibility to test for

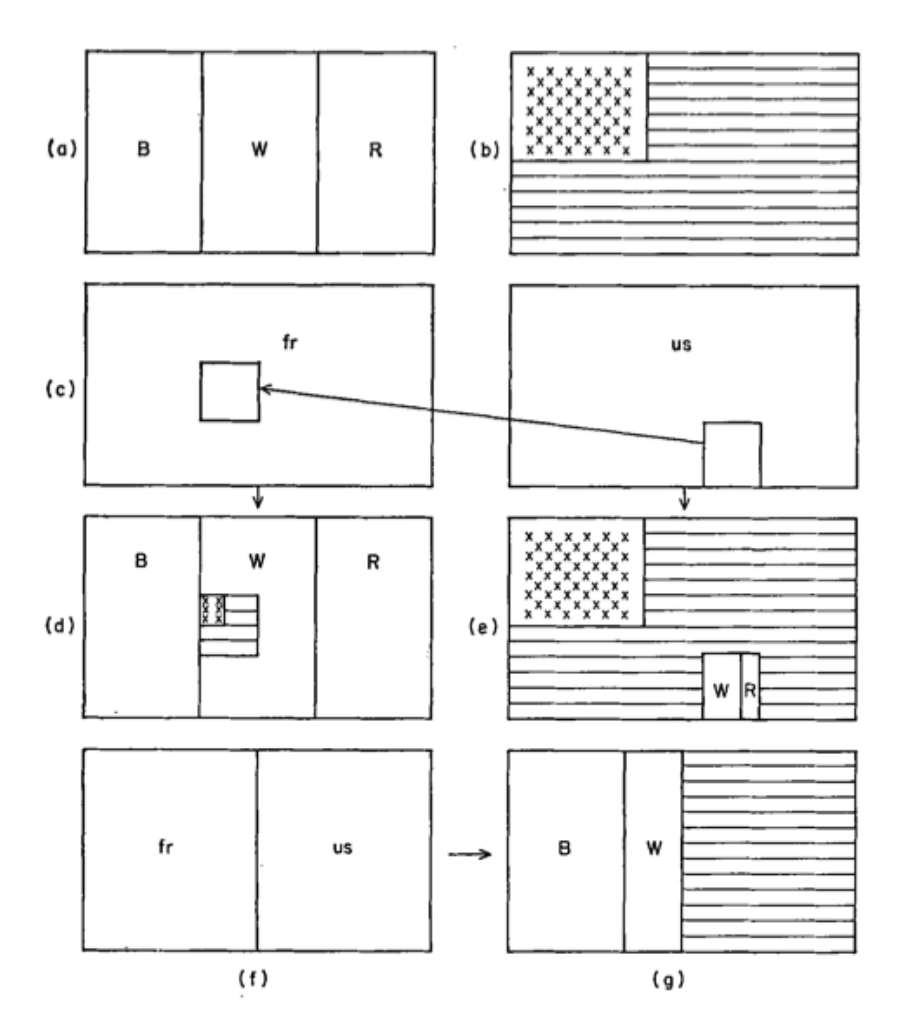


Figure 1–2: Morphogen gradients give positional information to the cell so that it can generate a pattern through differentiation. On the other hand, the gradient cannot change the outcome of a group of cells that are already predetermined to be of one type, e.g. French flag vs. US flag. a) The French flag pattern. b) The US flag pattern. c) ,d) e) grafting cells from the US to the French flag does not change their type, but changes their motif corresponding to their new position. f) g) Two halves of different types joined together lead to an hybrid flag. Figure reproduced as in *Positional Information and the Spatial Pattern of Cellular Differentiation* by Wolpert [7].

new dynamical models of development based on both temporal and positional factors. While the steady-state approach has been useful in explaining some aspects of development, there is much to be gained by considering the dynamical aspect of gene activation. For example, embryonic development can be broken down in stages whose relative duration is tightly controlled [9]. Meanwhile in somitogenesis, the segmentation clock driven by Wnt and Notch signaling controls the periodic formation of future vertebrae [10,11]. Periodic clocks are not

the only possible timing mechanism and there is evidence that many differentiation processes are at least partially controlled by the duration of exposure to some morphogens [12–14].

An interesting property of the French Flag Model is that positional information need not be given by the concentration of a morphogen. In reality, positional information can be acquired in many ways, one of which is the time of exposure to certain morphogens. In this temporal French Flag Model, Fig. 1–3, it is not only the concentration of morphogen, but the duration of exposure that specifies cell fate. We can imagine plotting the French flag, replacing the position axis by a time axis. Cells exposed for a short period become blue, cells exposed for a moderate period become white and cells exposed for a long period become red. The problem reduces to a matter of generating positional information from exposure time. This can be done for example by imagining that cells progressively migrate from a budding region, cells which leave early are exposed for shorter periods of time than cells which leave last. In such a way, we can generate a map between exposure time and cell position.

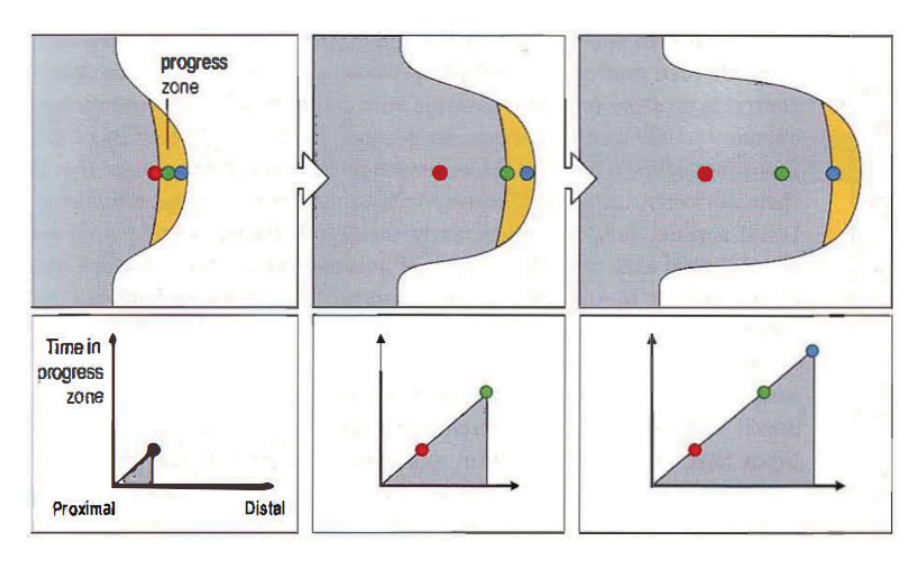


Figure 1–3: Morphogen gradients are typically used to interpret positional information. If positional information can instead be related to exposure time to a morphogen, one gets a Temporal French Flag Model. In the example of limb formation of Sec. 2.2, the time spent in the progress zone gives a relationship between position and exposure time as the limb grows along the proximal-distal axis. In the Temporal French Flag Model, the dynamics of gene expression cannot be ignored in favour of a steady-state description. Figure reproduced as in *Principles of Development* by Wolpert [6].

The problem then becomes one of finding a way for the cell to sense how long it has been exposed to a given morphogen. It is currently still unknown how such timing is performed by genetic and metabolic networks. One way could be through a timing variable [15, 16], effectively setting a time scale that could be used to capture temporal information. Models exist where a slowly accumulating protein plays the role of a slow variable which controls other faster variables. The faster variables quickly reach quasi-static equilibrium and become slaved to the slow variable [16]. Time of exposure then becomes a function of the concentration of the accumulating protein. Such timers have yet to identified, but experimental data suggests possible candidates.

However, recent experimental and computation results suggest a more elegant alternative. Rather than using an explicit timer, the timing mechanism could be an emerging property of the underlying gene regulatory network [14,17], whereby the interactions between genes give rise to a wide range of timescales much slower than the typical degradation rate.

1.3 Thesis Overview

Chapter 2 presents three examples from developmental biology from which we draw our inspiration. Sec. 2.1 is an overview of the Hox genes, the lessons to keep in mind is the existence of the various Hox clusters and the outcome of gene knocking out. Sec. 2.2 provides a biological context to the application of a Temporal French Flag model. Sec. 2.3 presents the network which sparked our interest in the emergence of timescales and their role in patterning.

In Chapter 3 we review the theory of GRNs and the tools available to us. In Sec. 3.1 we define gene networks and the equations that govern their interactions. In Sec. 3.2-3.4 we review dynamical systems theory and the tools it provides to study the dynamics associated with the a given GRN. Sec. 3.5 addresses the difference between deterministic and stochastic realizations of a GRN. We define the Langevin equation which we will use to probe the question of noise robustness.

We present our results in Chapter 4 starting with the setup used to simulate pattern formation given temporal morphogen signaling. We then, in Sec. 4.2 through Sec. 4.3 analyse and give analytical solutions to the GRN proposed by Balaskas et. al. [14, 17]. In Sec. 4.4 we generalize the GRN to an arbitrary number of genes and show how locally the

two networks are the same. Finally in Sec. 4.6 and onwards, we explore the effect of noise using the tools presented in Sec. 3.5.

Finally, in Chapter 5, we discuss the evolvability and emergence of timescales as a result of the GRN interactions. In Sec. 5.2 we contrast our model with previous models using explicit timers and describe how network duplication can lead to the behaviour seen in Hox genes expression. We conclude with Sec. 5.3 where we describe the future work to be done and the open questions that remain.

Two appendices are included at the end. Appendix A is an overview of the evolution algorithm used for parameter selection. We present two types of fitnesses which are used to select for domain patterning and noise robustness respectively. Appendix B presents a five dimensional network obtained via *in silico* evolution under the action of a temporal morphogen signal.

Chapter 2 - MOTIVATION

In this chapter, we provide a little bit of biological context to illustrate how the principles we study relate to development. We begin with an introduction to Hox genes and some of their properties. We later review how the formation of the chick limb can be an example of a temporal French Flag Model. We conclude with the work of Balaskas et al. [14,17] which probes the timing mechanism of neural tube patterning.

2.1 Hox genes

The Hox genes [18] are a large family of genes that share a DNA sequence known as the homeobox¹. They were historically discovered through mutations that led to one structure being transformed into another. For example, a mutation in the fly *Drosophilia* leads to a segment that does not bear wings to be replaced by a wing bearing segment resulting in a fly with two pairs of wings [19].

The Hox genes are grouped in clusters [20,21] which presumably come from duplication of an ancestral cluster. Vertebrates share many of these clusters on their chromosomes. For example, humans have four clusters: Hox A, HoxB, HoxC and HoxD on chromosomes 7, 17, 2 and 12 respectively. In mouse (Fig. 2–1), those clusters are located on chromosomes 6, 11, 15 and 2. Duplicated genes are knowns as paralogs and the corresponding group of genes across clusters is called a paralogous subgroup. For example, Hoxa4, Hoxb4, Hoxc4 and Hoxd4 form a paralogous subgroup in the mice. Not all paralogous subgroup span all clusters so that in mouse, Hoxa1, Hoxb1 and Hoxd1 form a paralogous subgroup in which there is no Hoxc1.

One interesting property of the Hox gene is colinearity. In many organism, but not all [21], the Hox genes are expressed sequentially in the embryo in the same order as they appear along DNA. See Fig 2–1. This cascading sequence of gene expression is a property we want to model as a function of time. We want to construct a gene network in which

¹ From which they derive their name, HOmeoboX.

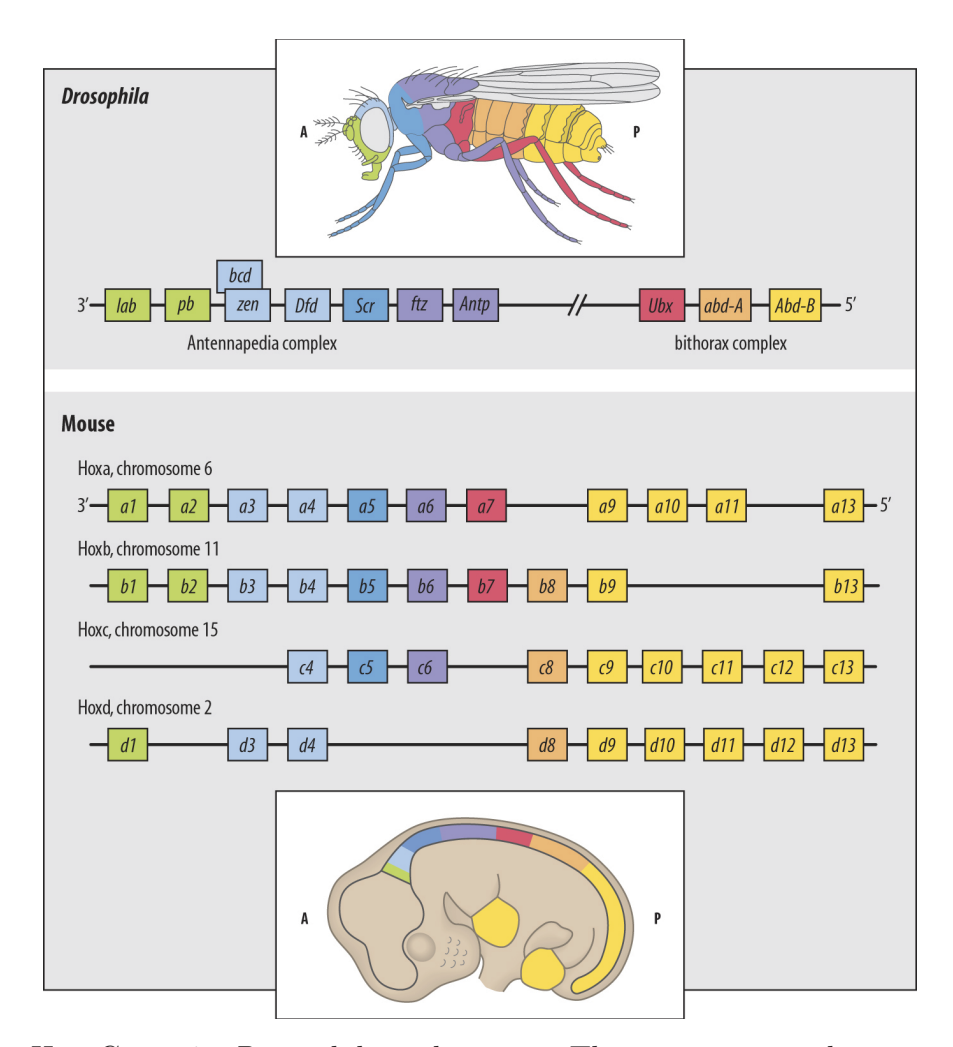


Figure 2–1: Hox Genes in *Drosophila* and mouse. They are expressed sequentially in the same order as they appear along DNA and color coded according to the regions they are responsible for. The Hox genes are ancestral and common to many organisms, such as the fruit fly and mice, through their duplication. Hox genes in the same column form a paralogous subgroup and those in the same row form a cluster. Figure reproduced as in *Principles of Development* by Wolpert. [6]

genes are sequentially activated such that stabilization after a period of time depends on the current gene being expressed. The proximity of these genes on DNA and their sequential expression might be a clue as to the nature of their interactions.

These three properties together can be used to compare our models and formulate predictions. Insertional mutagenesis and gene knock-out are two techniques whereby a gene can be modified or removed to observe its importance and influence on the development of the embryo. One example is the deletion of Hoxc8 in mouse embryo. Mutants lacking Hoxc8 never survive more than a few days and have many abnormalities, the most obvious is the

development of an extra pair of ribs [22]. The first lumbar vertebra is transformed into a more anterior structure, a rib-bearing thoracic vertebra. This suggests that in the absence of a gene, the gene network is nonetheless able to express the anterior genes. The Hox clusters might provide a redundancy in development which allows a modified gene network to retain some functionality. We explore this idea in the discussion of Chapter 5.

2.2 The formation of the limbs in chick embryo

The formation of the limbs in vertebrates is a prominent example of how the dynamical nature of developmental may come into play. Because the pattern is simple and easy to probe by surgical means, the chick limb is a good model for studying pattern development and inter-cellular signaling. By the third day after the egg is laid, the chick embryo develops limb buds which will lay out the structure of the limb (cartilage, muscles and tendons) within the next seven days [23].

At the tip of the limb bud is a thickening of the ectoderm called the apical ectodermal ridge, or simply the apical ridge. The progress zone is a region beneath the ridge in which undifferentiated mesenchymal cells reside. As those cells leave the progress zone, they differentiate into the cartilaginous structure that will later develop into the bones of the limb (in order, the humerus, radius and ulna, the carpas and the digits). The amount of time they spend in the progress zone is theorized to play a role in deciding the cell fate [24]. The proximal-distal axis is the axis that runs along the limb. As the limb grows, cells most proximal appear in the mesenchyme and leave the progress zone which migrates away from the body as the limb grows in length, Fig 2–2. The apical ridge stays further along the distal axis and the polarizing region (also called zone of polarizing activity, ZPA) which specifies position along the anterior-posterior axis is located along the limb on the posterior side, Fig. 2–2.

Many manipulations can be done on the limb bud without altering the resulting pattern, however both the apical ridge and the polarizing region are necessary for the correct pattern development. Grafting the ZPA on the other side of the limb bud leads to a mirroring of along the proximal-distal axis [25], while early ablation of the apical ridge leads to incomplete limbs with the most distal structures truncated [26]. This effect is countered if beads releasing

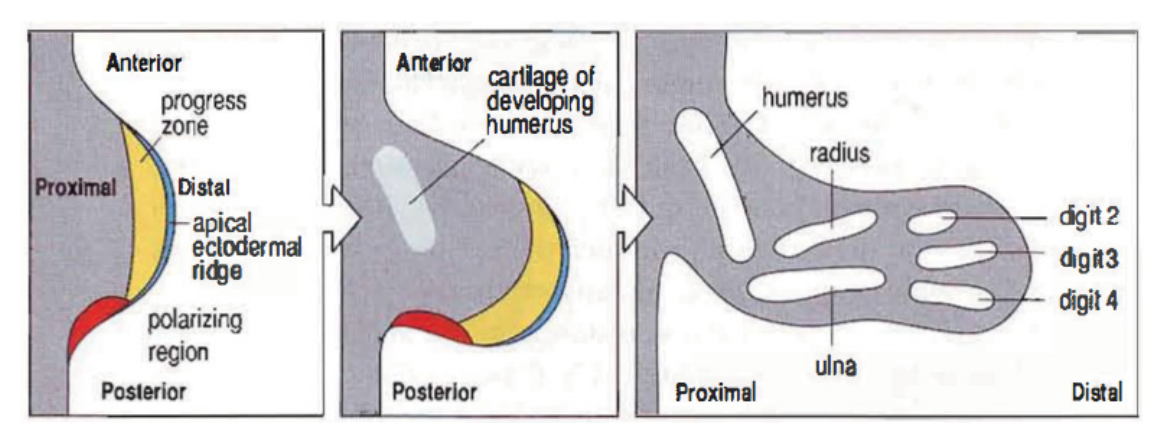


Figure 2–2: The polarizing region and the apical ectodermal ridge in the developing limb bud. The polarizing region (ZPA) together with the apical ridge are in a feedback loop maintaining their expression levels. The ZPA provides the positional information along the anterior-posterior axis while the apical ridge is thought to specify position, via time spent in the progress zone, along the proximal-distal. The formation of the humerus, radius, ulna and the carpals is sequential in time. Figure reproduced as in *Principles of Development* by Wolpert [6].

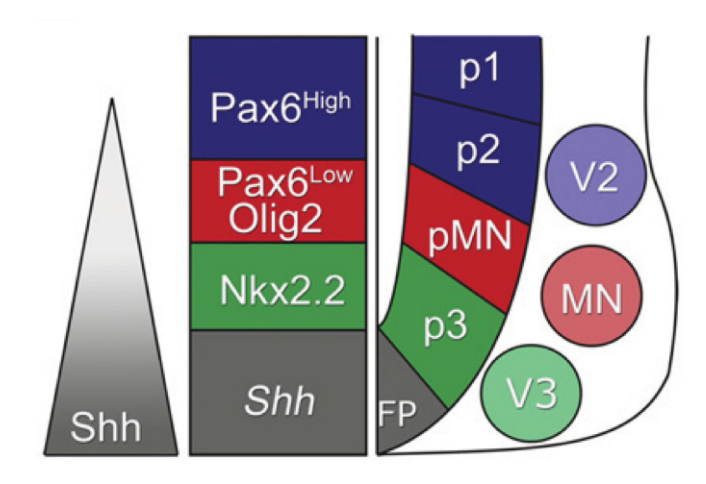
the growth factor FGF-4 are grafted in place of the apical ridge [27]. Sonic HedgeHog in the polarizing region and FGF-4 in the apical ridge are in a positive feedback loop which maintains their expression [28]. Thus the duration of exposure to morphogens [12,13] in the progress region leads to patterning along the embryo. If the exposure time is cut short, more distal structures cannot develop and the limb is abruptly terminated [26,29]. The position of the structure depends on the time spent in the progress zone and gives rise to a temporal French Flag Model as in Fig. 1–3.

We will model this type of time dependency in Sec 4.1 and use this mechanism to generate a patterned embryo with a temporal French Flag Model where the cell position is in direct correspondence with the exposure time to some morphogen.

2.3 A simplified model for neural tube patterning

As an additional example of a biological process where a static positional morphogen gradient is not enough to explain patterning [30,31], we introduce a model used by Balaskas et al. [14,17] to explain neural tube patterning guided by Sonic HedgeHog (Shh). In the vertebrate central nervous system, Shh protein controls the formation of five neural progenitor domains from the ventral neuroepithelium [32]. Increasing concentration of Shh ligand

or increasing activity of Gli (regulated by Shh) leads to successively more ventral neutral fates [30,33]. In addition, the duration of Shh signaling plays a role in the subtype identity of the neural progenitor domains such that longer exposure to Shh signaling is necessary for more ventral neural progenitor identities. As per Fig 2–3, these neural progenitor domains and identities correspond to the expression of three transcription factors Pax6 (P), Olig2 (O), Nkx2.2 (N) of which O and N are activated by Gli3 (G) which varies in time [33–35].



Gli(G) through the Figure 2–3: Shh gradient originating from floor plate (FP) leads the patterned gene expression of Pax6(P), Olig2(O), Nkx2.2(N).In turn, their level leads to the formation of the progenitor domains (p1,p2,p3,pMN) which eventually generate distinct neuronal subtypes (V2,MN,V3). Figure reproduced as in Gene Regulatory Logic for Reading the Sonic Hedgehog Signaling Gradient in the Vertebrate Neural Tube by Balaskas et al. [14]

Balaskas et al. offer a model of the interactions between these transcription factors which successfully explains how the duration of Shh signaling is interpreted by the network to produce the neural progenitor domains. Figure 2–4. summarizes the interactions and Eq. 2.1 is the mathematical relationship for their expression². The early P represses the late N, O represses P and N, N represses O and P, and finally G activates N and O, but not P.

² Note that the notation and the corresponding ODEs do not agree with the convention we adopt in Sec. 3.1. The difference in behaviour is negligible.

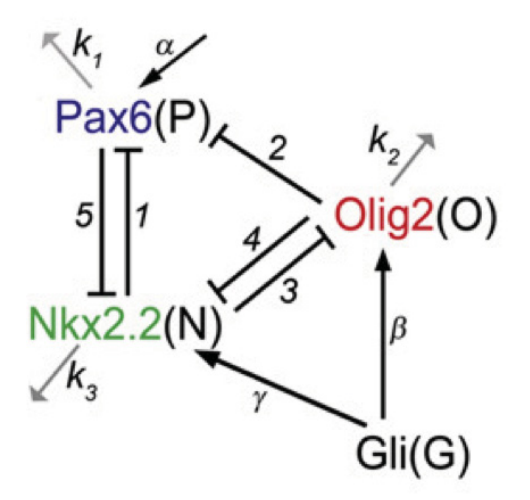


Figure 2-4: GRN representing the interactions between Nkx2.2(N), Olig2(O), Pax6(P)and Gli(G) through Shh(S). Flat arrows are repression and normal arrows are activation. Figure reproduced as in Gene Regulatory Logic for Reading the Sonic Hedgehog Signaling Gradient in the Vertebrate Neural Tube by Balaskas et al. |14|

$$\dot{P} = \frac{\alpha}{1 + \left(\frac{N}{N_{critP}}\right)^{h_1} + \left(\frac{O}{O_{critP}}\right)^{h_2}} - k_1 P$$

$$\dot{O} = \frac{\beta G}{1 + G} \times \frac{1}{1 + \left(\frac{N}{N_{critO}}\right)^{h_3}} - k_2 O$$

$$\dot{N} = \frac{\gamma G}{1 + G} \times \frac{1}{1 + \left(\frac{O}{O_{critN}}\right)^{h_4} + \left(\frac{P}{P_{critN}}\right)^{h_5}} - k_3 N$$
(2.1)

This model is of particular interest to us because a timescale emerges from the property of the network whereby a transition from $P \to O \to N$ successively happens (Fig. 2–5) in time and eventually leads to five domains,. Upon careful examination, this timescale is found to be controlled by the concentration of G, or alternatively by parameters mediating the activation of O and N by G (parameters not considered in the formulation given by Balaskas et al.). The full details of the analysis are considered in Chapter 4 and we will generalize this type of gene network to simulate patterning with a temporal French Flag Model for greater number of genes.

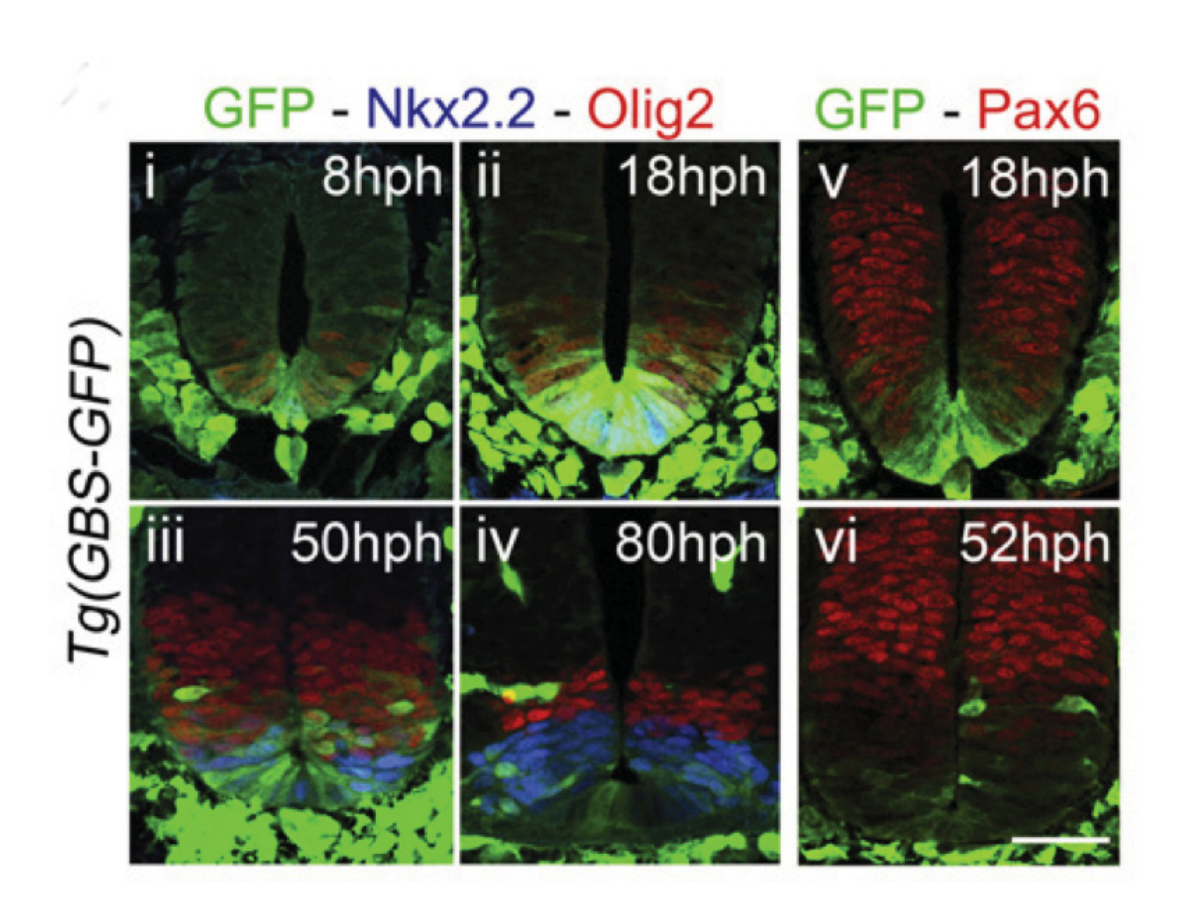


Figure 2–5: Fluorescence of O, N and P at different stages of neural tube patterning. The gene expression levels change in time and there is a transition from $P \to O \to N$. Figure reproduced as in Gene Regulatory Logic for Reading the Sonic Hedgehog Signaling Gradient in the Vertebrate Neural Tube by Balaskas et al. [14]

Chapter 3 - Dynamical system theory for Gene Regulator Networks

3.1 Genes Regulatory Networks (GRN)

Proteins are complex macromolecules involved in virtually all processes within the cell. Specific proteins direct molecules to their rightful place, others act as enzymes catalyzing important reactions, some even directly influence the very process by which they are transcribed. We call the aggregate of proteins, DNA, RNA and the various other molecules involved a Gene Regulatory Network (GRN). Many approaches exist to the modeling of GRNs and we shall give a brief introduction to some notable formalisms.

In the context of developmental biology and cell fate, it is possible to classify cells by attributes such as their function, position and composition. It is also possible to collect data regarding the various genes being expressed in a given cell type. Together these two variables can be used to form some sort of table cataloging the different cells and their respective genes distribution. From this table, one can compute correlations of various orders between distinct cell types and genes. One can use this type of data to model genes as being part of a network of interacting nodes. Like in an Ising model [36], where the spin of an electron can be either up or down, a gene can either be on or off according to some threshold concentration. Interactions between genes can be modeled as a favourable or disfavourable change in the energy E(C) of a configuration $C = \{g_1, g_2, g_3, \ldots, g_N\}$ where $g_i \in \{+1, -1\}$. If we only allow two point interactions, E(C) is given by eq. 3.1

$$E(C) = \frac{1}{2} \sum_{i,j} J_{ij} g_i g_j + \sum_i h_i g_i$$
 (3.1)

The cell fate can then be defined as a configuration C that is a local minimum of E(C) and the strength of the interactions J_{ij} , h_i can be inferred from the data table of cell types and gene expression. The network can be made time dependent if we update the network every time step τ by changing g_i according to some rule based on C. This type of Ising model has been successfully applied to other fields of biology, notably the Hopfield network [37] in the context of memory and neural networks. This type of approach tends to be very

high dimensional, there are thousand of genes in an organism (or alternatively billions of neurons in the human brain) and the method offers a very coarse insight on the nature of gene interactions. The same types of generalizations that apply to the Ising model tend to be applicable in biology, for example, as a type of Potts model [38], the genes g_i could take on a wider range of values than $\{+1, -1\}$. It is also possible to take into account higher order interactions of the form $\frac{1}{n!} \sum_{i_1,i_2,...,i_n} w_{i_1i_2...i_n} g_{i_1} g_{i_2} \dots g_{i_n}$ in Eq. 3.1.

A more detailed approach consists in making a biologically faithful model of interactions while remaining simple enough to be computationally useful. By modeling gene expression as a set of coupled ordinary differential equations (ODEs) [39], either deterministically or stochastically, one can work with variables $G_i(t)$ representing the time dependent concentration of various genes. The steady-state of the ODEs is used to represent the potentially viable fate of the cell and many phenomena arise from the complex solutions to these ODEs. We are particularly interested in the time dependence of gene expression and how the transient behaviour can be used in the context of development [40].

A gene interacts with another through extra terms acting on the production rate of the affected gene. The effect of morphogens is encapsulated in additional variables $M_j(t)$ whose values are externally fixed as a function of time. Their interactions are also described as changes in the gene's production rate. Gene networks can be mathematically transcribed into an equation of the form

$$\frac{dG_i}{dt} = P_i(M_1, M_2, \dots, M_n, G_1, G_2, \dots, G_N) - \lambda_i G_i$$
(3.2)

where P_i is the production term and $\lambda_i G_i$ is the degradation term with λ_i the associated degradation rate. The usual form of P_i is either assumed based on a phenomenological model or can be given by Law of Mass-Action which serves to predict the behaviour of chemical solutions in dynamic equilibrium. The P_i 's are usually taken as low order polynomials or products of Hill functions (see Eq. 3.4 for a concrete example).

$$\operatorname{Hill}(G, T, h) = \frac{1}{1 + (G/T)^h} = \begin{cases} \frac{T^h}{T^h + G^h} & \text{if } h > 0, T > 0\\ \frac{G^h}{T^h + G^h} & \text{if } h < 0, T > 0\\ 1 & \text{if } h = 0, T = 0 \end{cases}$$
(3.3)

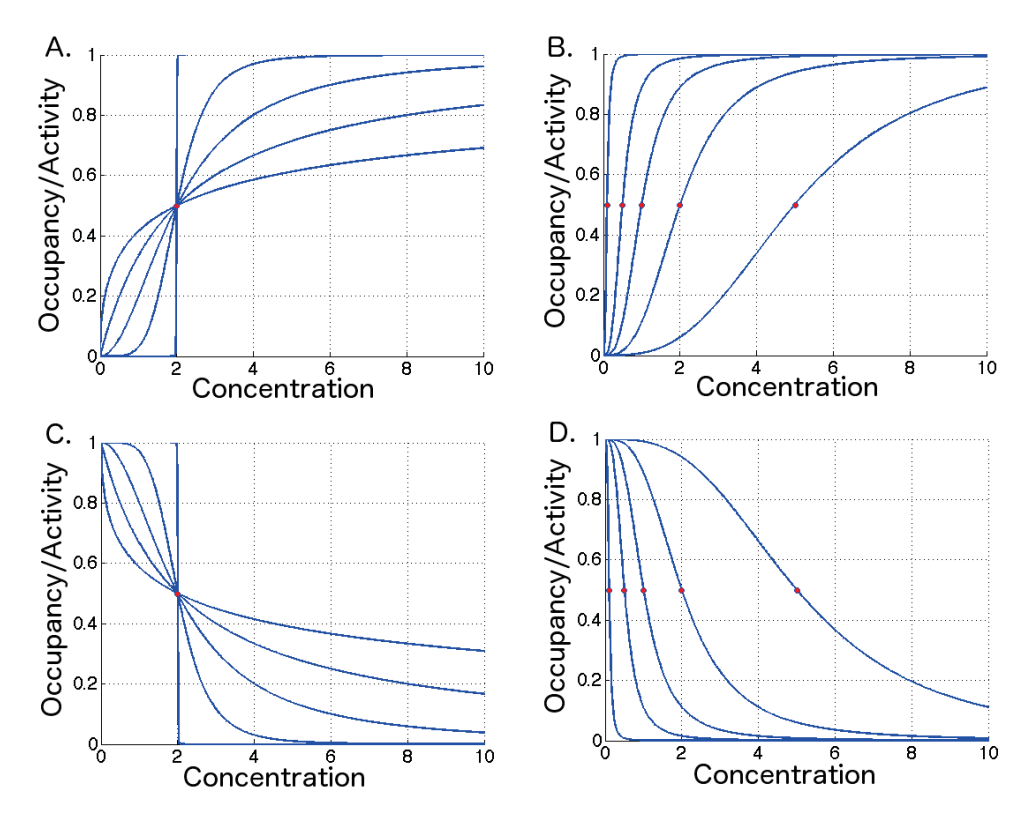


Figure 3–1: Example Hill functions for gene activation or repression. Red dots correspond to half occupancy/activity. A. Activation with h = -0.5, -1, -2, -5, -400 and T = 2 from left to right respectively. B. Activation with h = -3 and T = 0.1, 0.5, 1, 2, 5 from left to right respectively. C. Repression with h = 0.5, 1, 2, 5, 400 and T = 2 from left to right respectively. D. Repression with h = 3 and T = 0.1, 0.5, 1, 2, 5 from left to right respectively.

Eq. 3.3 is the Hill function and is most notably used in the context of ligands binding [41]. It describes the fraction of ligands bound as a function of ligand concentration. G > 0 is usually the ligand concentration, T > 0 is the ligand concentration producing half occupancy and h is the Hill coefficient¹ describing the cooperativity. -1 < h < 0 denotes negative cooperativity, h < -1 is positive cooperativity and h = -1 is non-cooperative binding.

However, in the context of gene networks, Hill functions are also used to describe activation and repression of genes as was shown in the case of Hunchback and Bicoid [42]. In that context, G > 0 is the concentration of the gene acting on the production rate of another gene. T > 0 is the threshold of concentration halving the production and h is the Hill

¹ Eq. 3.3 is sometimes defined as $\frac{1}{1+(T/G)^h}$ in which case the Hill coefficients h are the negative of those we present.

coefficient describing the strength (steepness of the curve) of the activation or repression. A positive Hill coefficient corresponds to repression, i.e. gene G impedes the production, while a negative Hill coefficient corresponds to activation, i.e. the gene catalyzes the reaction. In the limit $h \to \pm \infty$, the Hill function converges to the Heavyside function which is either zero or one with a sharp transition at G = T. We take the convention that h = 0, T = 0 leads to no effect on the production. Figure 3–1 shows four families of Hill functions with varying parameters.

Gene networks graphs are used to represent genes and their interactions. Genes and morphogens are represented as nodes and interactions are edges. Nodes are sometimes codified by shape to differentiate between morphogens (inputs), genes that are outputs (realizator genes) and regular genes (genes which interact with the outputs but are not outputs themselves). Arrows running from G_1 to G_2 represent activation of G_2 by G_1 , flat-headed arrows from G_1 to G_2 represent repression of G_2 by G_1 . An arrow from a node to itself represents self-activation or self-repression. It must be noted that these interactions are not faithful representations of reality, but instead effective interactions averaging over the details to simplify the model. In reality it is not the genes that activates or represses other genes, instead a gene, say G_1 codes for a certain protein which in turn affects the complicated process of DNA transcription thereby changing the rate at which G_2 is transcribed. The process is abstracted as an interaction between G_1 and G_2 through the Hill function.

Figure 3–2 shows a gene network graph with a legend to illustrate the convention. Figure 3–2 B. also shows the steady-state concentration of the genes of an array of cells (represented by the position axis). Each cell is exposed to different concentration of the input morphogen 0 which leads to patterning into three separated domains. The parameters and the topology of the network (i.e. the way in which the edges relate to the nodes) determine the resulting pattern.

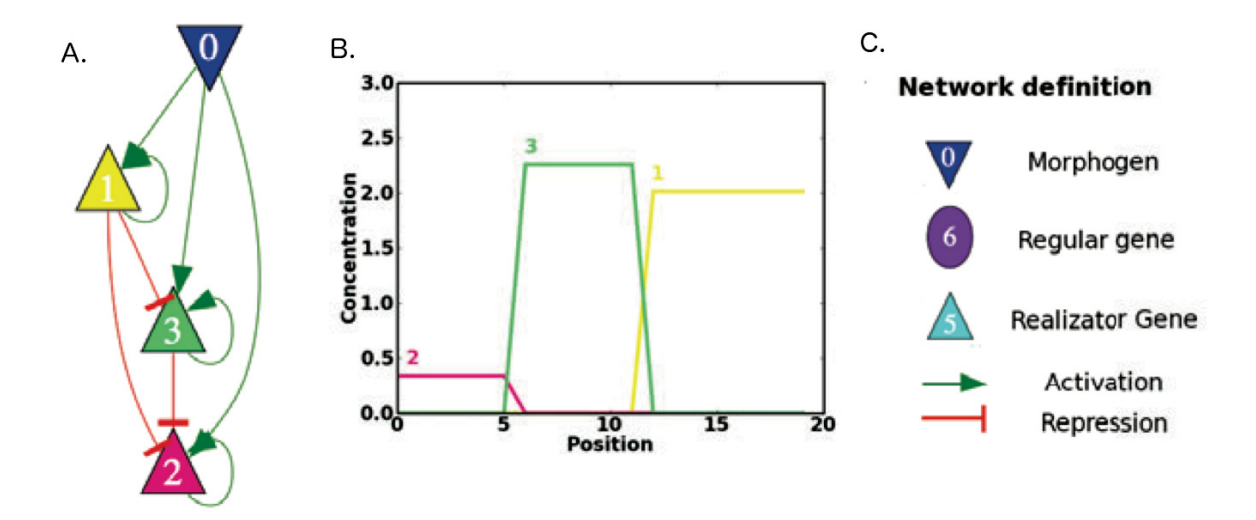


Figure 3–2: Graph and Output for an example GRN. A. Graph of genes and corresponding interactions. B. Output of an array of cells (same GRN) denoted by position. Each cell is subjected to a different morphogen profile leading to distinct fates represented by the three domains. C. Legend corresponding to the GRN graph. The figure is reproduced as in Francois, Siggia, 2010 [16].

$$\begin{split} \frac{dG_1}{dt} &= \alpha_1 \max\{\text{Hill}(M, T_{1M}, h_{1M}), \text{Hill}(G_1, T_{11}, h_{11})\} - \lambda_1 G_1 \\ \frac{dG_2}{dt} &= \alpha_2 \max\{\text{Hill}(M, T_{2M}, h_{2M}), \text{Hill}(G_2, T_{22}, h_{22})\} \text{Hill}(G_1, T_{21}, h_{21}) \text{Hill}(G_3, T_{23}, h_{23}) - \lambda_2 G_2 \\ \frac{dG_3}{dt} &= \alpha_3 \max\{\text{Hill}(M, T_{3M}, h_{3M}), \text{Hill}(G_3, T_{33}, h_{33})\} \text{Hill}(G_1, T_{31}, h_{31}) - \lambda_3 G_3 \end{split}$$
(3.4)

Eq. 3.4 is the set of coupled ODEs corresponding to the GRN of Fig. 3–2. α_i, λ_i is the production rate, degradation rate of G_i respectively. T_{ij}, h_{ij} are the parameters of the Hill function parameterizing the effect of G_j on G_i . Similarly, T_{iM_j}, h_{iM_j} parametrize the effect of the morphogen M_j on G_i . In the case of repression i.e. $h_{ij} < 0$, each Hill function multiplies the rate. In the case of activation, only the maximum of the activating Hill functions multiplies the rate, the catalyst effectively compete with each other and the strongest effect is felt. The general equation relating all the interactions is given by Eq. 3.5. Compare with Eq. 3.4 and the interactions of Fig. 3–2.

We now introduce a matrix notation to store hill parameters in a compact way and show case interactions. Eq. 3.5 is the general ODE that can be constructed given a full set of parameters (of which some might be zero, representing no interaction). Once familiar, these matrices immediately tell us how each gene is affected by the other genes. Table 3–1 summarizes Eq. 3.4 in accordance with Eq. 3.5 for the GRN of Fig. 3–2. The sign of h_{ij}, h_{iM_j} is made explicit through the use of absolute value.

Rates				
	G_1	G_2	G_3	
Production α	α_1	α_2	α_3	
Degradation γ	γ_1	γ_2	γ_3	

Hill Coefficients						
	G_1	G_2	G_3	M		
G_1	$- h_{11} $	0	0	$- h_{1M} $		
G_2	h_{21}	$- h_{22} $	h_{23}	$- h_{2M} $		
G_2	h_{31}	0	$- h_{33} $	$- h_{3M} $		

Thresholds						
	G_1	G_2	G_3	M		
G_1	T_{11}	0	0	T_{1M}		
G_2	T_{21}	T_{22}	T_{23}	T_{2M}		
G_2	T_{31}	0	T_{33}	T_{3M}		

Table 3–1: Example table for the 3D GRN of Fig. 3–2.

$$\frac{dG_i}{dt} = \alpha_i \max_{\substack{h_{ij} < 0 \\ h_{iM_j} < 0}} \left\{ \text{Hill}(S_j, T_{i\{j,M_j\}}, h_{i\{j,M_j\}}) \right\} \prod_{\substack{h_{ij} \ge 0 \\ h_{iM_j} \ge 0}} \text{Hill}(S_j, T_{i\{j,M_j\}}, h_{i\{j,M_j\}}) - \lambda_i G_i$$
(3.5)

Where S_j stands for G_j or M_j with corresponding parameters $T_{i,\{j,M_j\}}, h_{i,\{j,M_j\}}$

3.2 Phase Space and Multistability

The phase space [43] is a mathematical tool which we borrow from physics to explain the dynamics of gene networks. In the phase space, each possible state of the system is represented by a point in a multidimensional space corresponding to the degrees of freedom of the system. As such, changing a variable (such as position or gene concentration) in the mathematical model corresponds to shifting along the dimension of that degree of freedom. If the variables depend on a parameter such as time and are constrained by a relationship or rule (such as the interactions in a GRN or the laws of motion in classical physics) then we can draw a curve through phase space depicting the state of the system as a function of time. The first order system of ordinary differential equations in vector form

$$\frac{d\vec{x}}{dt} = \vec{f}(\vec{x})$$

is an example of a relationship specifying the state $\vec{x}(t+dt)$ as a function of the previous state $\vec{x}(t)$. In classical physics, position q and momentum p are two degrees of freedom related through Newton's Laws of motion which specify a set of coupled first order differential equations to solve for the degrees of freedom as a function of time starting from an initial condition. Plotting the resulting trajectory on the phase space shows the evolution of the state (q(t), p(t)) compatible with the initial state $(q(t_0), p(t_0))$. A family of such curves can then be plotted for various initial states (p, q) to show the possible responses and outcomes of the system to be studied. Fig. 3–3 is the phase portrait of the non-linear pendulum for different energies where $(\theta, \dot{\theta})$ play the role of the canonical variables (q, p) [44].

The phase space often has specials points and trajectories. For example, In Fig. 3–3, the separatrix is the set of points which separates two regions of phase space with very different behaviour. Another special set of points are the nullclines associated to x_i which are defined as the states \vec{x}_{null} such that, for a given i,

$$\frac{dx_i}{dt} = f_i(\vec{x}) = 0.$$

Their intersection defines a fixed point, or alternatively steady state, a special state of the system which does not change as a function of time. A specific example is given in Sec.

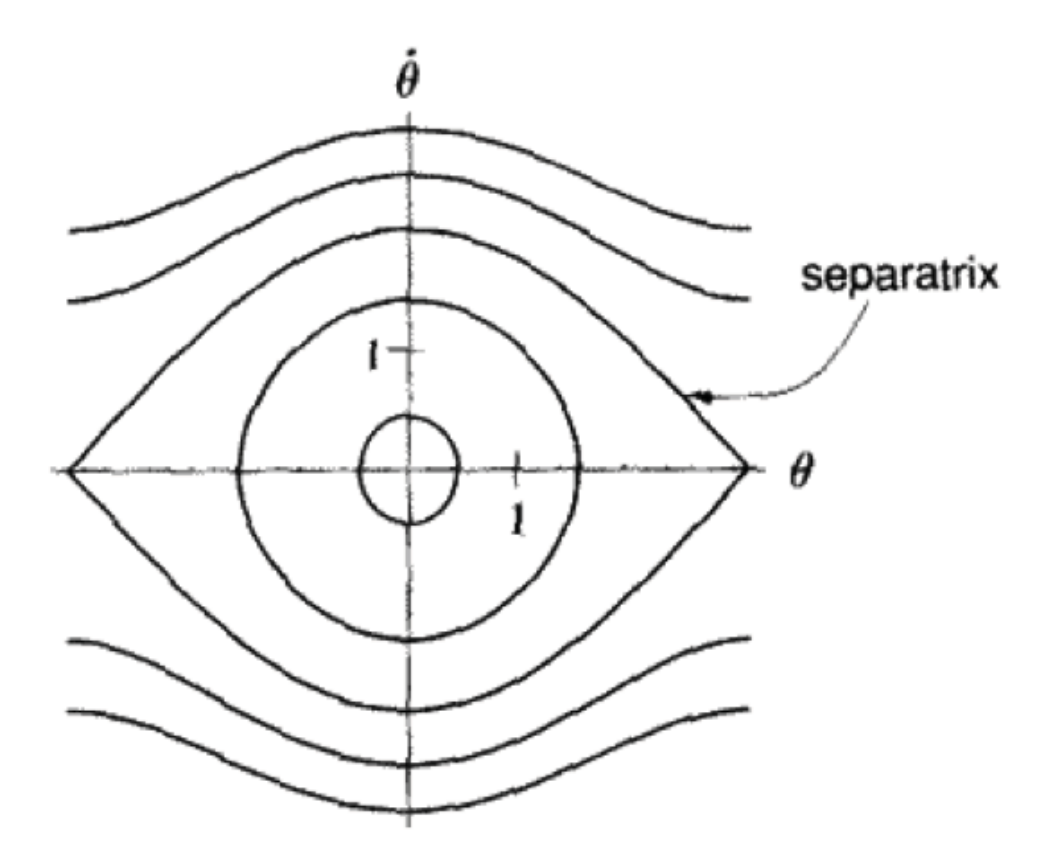


Figure 3–3: Phase portrait of the non-linear pendulum where $(\theta, \dot{\theta})$ play the role of the canonical variables (q, p). Because energy is conserved, each curve corresponds to a given energy. The separatrix is the boundary between rotations and liberation. The figure reproduced as in *Analytical Mechanics* by Hand & Finch. [44]

3.4 with the associated figure 3–4. Mathematically, those points are defined as any point \vec{x}^* satisfying the equation

$$\frac{d\vec{x}}{dt} = \vec{f}(\vec{x}^*) = \vec{0}$$

Fixed points can either be stable or unstable. A stable fixed point is one such that given a tiny perturbation of the state $\vec{x^*}$ into the state $\vec{x^*} + \delta \vec{x}$ converges back into the fixed point $\vec{x^*}$ in finite time. An unstable fixed point is one such that a tiny perturbation leads to a large change in the system's state away from the fixed point \vec{x}^* . A fixed point for which perturbations in different directions lead to both attractive and repulsive behaviour is also called a saddle. Mathematically, this behaviour can be captured by Taylor expanding around the fixed point and examining the eigenvalues of the resulting linear system Eq. 3.6

$$\frac{d\vec{x}}{dt} = \vec{f}(\vec{x}^* + \delta \vec{x}) \approx \vec{f}(\vec{x}^*) + \hat{A}(\vec{x}^*) \cdot \delta \vec{x}$$

$$\hat{A}(\vec{x}^*) = \frac{d\vec{f}}{d\vec{x}}|_{\vec{x}^*}$$
(3.6)

where \hat{A} is the Jacobian matrix whose columns are the gradients of the entries x_i of \vec{x} evaluated at the fixed point \vec{x}^* . The stability of \vec{x}^* in the direction of the eigenvector $\vec{v_i}$ can be read off from the corresponding eigenvalue λ_i of \hat{A} , negative eigenvalues are associated with a stable direction and positive eigenvalues with unstable directions. Complex eigenvalues come in pairs and are indicative of oscillations while zero eigenvalues are a special subject we will treat in the next section.

Stable fixed points are of particular importance to us and we will assume cell fates correspond to stable fixed points. Unstable fixed points are less relevant due to the effect of noise on the viability of such states. The phase space then corresponds to all states accessible to the cell, of which fixed points represent all possible cell fates. The set of initial conditions accessible to a cell further restrict which fixed points are realizable fates for a given cell. Multistability is then the mathematical statement that multiple fates can be sustained simultaneously in an environment and regulation is the act of driving cells to one fate over another.

As we mentioned above, complex eigenvalues lead to oscillation. In particular, they lead to limit cycles which can be either attractive or unstable depending on the sign of the real part of the eigenvalue. Oscillators are useful and can be used to model development of periodic structures, however oscillators are fundamentally different from fixed points in that they constantly change in time although in a predictable and regular manner. As such, to model cell fate as the steady state outcome of a GRN, we will require a method for oscillators to reach stability. It is a priori not obvious how GRN can give rise to oscillating genes in one regime (such a high concentration of a morphogen) while being multistable in another regime (low concentration of a morphogen).

3.3 Slow manifolds

We saw in section 3.2 that in order to assess the stability of a fixed point, it is necessary to look at the eigenvalues λ_i of the linearized system near the fixed point. We can define four linear invariant subspaces based on the eigenvalues λ_i of \hat{A}

- The stable subspace spanned by the generalized eigenvectors corresponding to the eigenvalues λ_i with $Re(\lambda_i) < 0$.
- The unstable subspace spanned by the generalized eigenvectors corresponding to the eigenvalues λ_i with $Re(\lambda_i) > 0$.
- The center subspace spanned by the generalized eigenvectors corresponding to the eigenvalues λ_i with $Re(\lambda_i) = 0$.
- The slow subspace spanned by the generalized eigenvectors corresponding to the eigenvalues λ_i with $\lambda_i = 0$.

From our definition, it is clear that the slow subspace is a, possibly empty, subspace of the center manifold. The behaviour of the center subspace cannot in general be described by the linearization of the system. Indeed, it is a sign that the quadratic or higher order terms play an important role. Center subspaces often arise in bifurcation theory and lead to interesting phenomena. The linearized subspaces play an important role in the theory of non-linear systems as they define tangent spaces to the invariant manifolds of the non-linear system.

We will focus on the slow manifold as a relevant object of study. It has numerous simplifying properties. Because of their zero eigenvalues, slow manifolds act as master variables upon which faster variables reach quasi-static equilibrium. Fast variables can therefore be 'integrated out' leading to a lower dimensional system approximating the original non-linear system [45–47]. Lower dimensional systems, by virtue of their comparable simplicity, tend to be easier to study and analytical result are more readily extracted. In this way, slow manifold theory can be used to simplify both ODE and PDE systems. Interestingly, the theory of slow manifolds has also been applied to stochastic systems in biology [48, 49], although there are considerably more subtleties such as the correlations between variables.

An important point that must be kept in mind is that a slow subspace is rigorously defined precisely at a fixed point \vec{x}^* with one or many eigenvalues λ_i precisely equal to zero.

Despite this, slow manifold theory can sometimes successfully be used near a fixed point provided slow and continuous changes in phase space, in which case the constant term in the Taylor expansion is non zero, yet sufficiently small. Fast variables can also be eliminated even in the case $\lambda \approx 0$ as long as there is a clear separation in magnitude compared to the other eigenvalues.

3.4 Bifurcation theory

Bifurcation theory is the study of topological changes in families of curves as a result of infinitesimal parameter variation. A family of curves could be, for example, the solutions to a differential equation while a topological change might be the apparition of fixed points or limit cycles. The parameter to be varied could be the mass of an object, the concentration of a morphogen or the production rate of a protein. Bifurcation diagrams, like that of Fig. 3–5, are plots of the fixed points as a function of the bifurcation parameter. They serve to illustrate the topological change that can happen at critical values of the bifurcation parameter.

Bifurcations come in two kinds, local and global. A local bifurcation can be analyzed through changes in the local stability of fixed points. They are limited small regions of phase space as the bifurcation parameter is smoothly changed. Global bifurcations, on the other hand, lead to changes in topology that extend to arbitrary large distances. They cannot be studied through the local stability of fixed points.

We will focus on local bifurcations. The most well known local bifurcations are saddle-node, pitchfork and Hopf bifurcations. In the saddle-node bifurcation, two fixed points, one stable and one unstable, collide and disappear leaving no trace as the bifurcation parameter is varied. In a pitchfork bifurcation, the number of fixed points locally goes from one to three, preserving the the number of stable fixed points minus the number of unstable fixed points. In a Hopf bifurcation, a shrinking limit cycle collides with a fixed point and disappears. If the fixed point is attractive, the limit cycle is unstable and vice versa.

In the present work, we will deal exclusively with saddle node bifurcations, thus we give a simple biological example, a switch [50]. Let x be the concentration of a protein and y

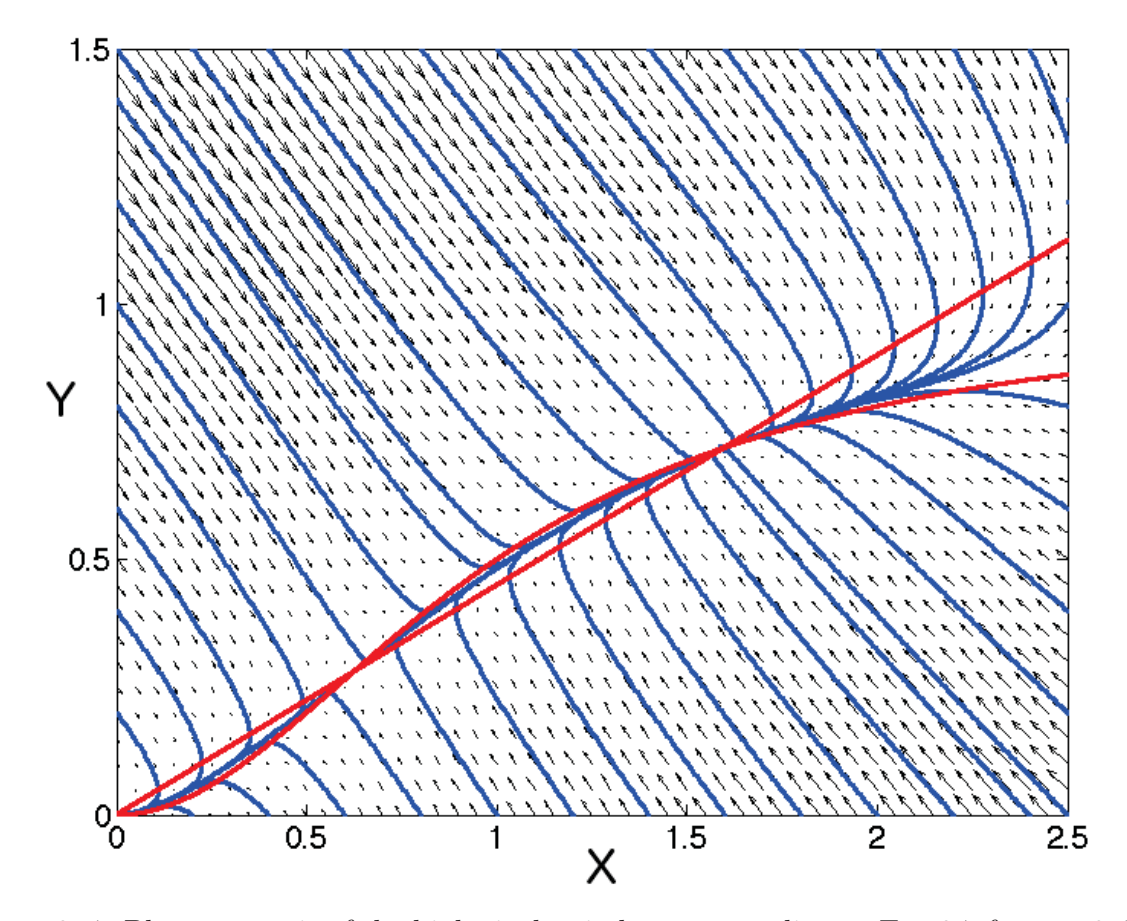


Figure 3–4: Phase portrait of the biological switch corresponding to Eq. 3.7 for a = 0.45, b = 1. The black arrows indicate the direction and magnitude of the flow. The blue lines are families of curves tangent to the arrows. The red lines are the nullclines given by Eq. 3.8 which intersect in three points corresponding to the fixed points.

the concentration of mRNA translating a gene. Let the gene produce protein x and let x activate the gene. In dimensionless form, this leads to the following ODEs:

$$\dot{x} = y - ax$$

$$\dot{y} = \frac{x^2}{1 + x^2} - by$$
(3.7)

where a > 0 and b > 0 are degradation rates. The system is either stable or bistable after undergoing a saddle-node bifurcation. To see this, observe the nullclines in Fig. 3–4 given by Eq. 3.8.

$$0 = y - ax \qquad \rightarrow y = ax$$

$$0 = \frac{x^2}{1 + x^2} - by \qquad \rightarrow y = \frac{x^2}{b(1 + x^2)}$$

$$(3.8)$$

To find where the nullclines intersect, we solve the equation $ax = \frac{x^2}{b(1+x^2)}$ for which $x^* = 0, y^* = 0$ is a always solution. Assuming $x \neq 0$, we only need to solve the quadratic equation $ab(1+x^2) - x = 0$ to get the remaining roots. The solution is then

$$x_{\pm}^* = \frac{1 \pm \sqrt{1 - 4a^2b^2}}{2ab}, \qquad x^* = 0$$

 $y_{\pm}^* = \frac{1 \pm \sqrt{1 - 4a^2b^2}}{2b}, \qquad y^* = 0$

There are two solutions when the discriminant is positive, i.e. 2ab < 1. If we vary a, the bifurcation happens when $a_c = \frac{1}{2b}$, past the bifurcation x_+^* corresponds to the stable fixed point and x_-^* corresponds to the unstable fixed point, $x^* = 0$ is always stable. The bifurcation diagram Fig. 3–5 shows the annihilation of the two fixed points at $a_c = 0.5$ for b = 1.

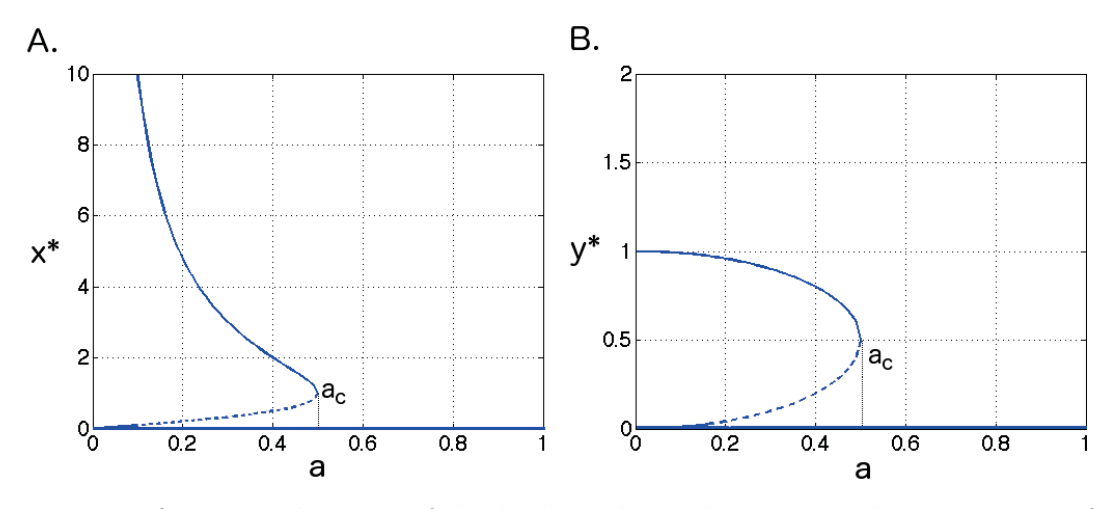


Figure 3–5: Bifurcation diagram of the biological switch corresponding to Eq. 3.7 for b=1 as a is varied past $a_c=0.5$. Full lines are stable fixed points and dashed lines represent unstable fixed points. The two fixed points collide at $a_c=0.5$ leaving only x*,y*=0 as a stable fixed point. A. shows the x-component of the stable fixed points and B. shows the y-components.

3.5 Langevin Equation and Tau Leaping

So far we have only considered deterministic equations, however, biological systems tend to be very noisy [51]. Without robust models [52] that take into account the stochastic nature of chemical reactions, there is little hope to describe development accurately and many phenomena can be missed [53]. The effective number of reacting molecules tends to be relatively low, sometimes as low as ten molecules as in the case of ligands in the immune system. With such low numbers of molecules, stochastic approaches are necessary to get realistic results. The effect of noise in development might be so great as to prohibit or favor certain types of interactions [54, 55]. It sets an effective upper bound on how accurately information can be inferred from biological quantities [56]. In particular, it was shown that GRNs are not limited to "on/off" states and can carry information greater than one bit even in the presence of noise [57].

In essence, the most general way to model a stochastic system is by writing out every possible state and assign probabilities to transition from one state to another. The probability distribution is then the solution of the Master Equation [58], the equation that relates every state to another. One can try to solve the Master Equation, but unless one is working with the simplest systems, there is little hope for an analytic solution. The Fokker-Planck equation, a PDE which serves as a continuous approximation to the Master equation can sometimes be solved such as in the case of the continuous Wiener process, but often time the only hope is to numerically tackle the problem.

A stochastically faithful algorithm was given by Gillespie [59], it generates accurate realizations of a noisy system. However, the exactness of the simulation comes at great computational cost. The chemical Langevin equation is a stochastic differential equation which approximates the Master Equation and is equivalent to the Fokker-Planck equation. It treats the stochastic system as being a deterministic system with a noise driven force. For a single species which can undergo M reactions, the chemical Langevin equation is:

$$\frac{dX(t)}{dt} = \sum_{j=1}^{M} \nu_j a_j(X(t)) + \sum_{j=1}^{M} \nu_j \sqrt{a_j(X(t))} \Gamma_j(t)$$
 (3.9)

where X(t) is the chemical specie, ν_j is the stoichiometric coefficient of reaction j, a_j is the propensity function which regulates the effect of X(t) and Γ_j is uncorrelated Gaussian white noise obeying

$$\langle \Gamma_j(t), \Gamma_{j'}(t') \rangle = \delta_{jj'} \delta(t - t')$$

Eq. 3.9 can be numerically integrated using the Tau Leaping method [60]. Taking time steps τ , we can perform the Euler method with the iterative equation

$$X(t+\tau) = X(t) + \sum_{j=1}^{M} \nu_j a_j(X(t))\tau + \sum_{j=1}^{M} \nu_j \sqrt{a_j(X(t))} \sqrt{\tau} \,\tilde{\Gamma}_j(\mu = 0, \sigma = 1)$$
 (3.10)

where $\tilde{\Gamma}_j(0,1)$ is a Gaussian with mean zero and standard deviation one. τ here must be small enough that the propensity functions a_j do not change much. At the same time τ cannot be too small, it must be big enough that all reactions fire multiple times within time τ .

In this thesis, we will stick to GRN and limit ourselves to a production term $\vec{f}(M, \vec{x})$ regulated by a morphogen M and a degradation term $\vec{g}(\vec{x})$. We work with \vec{x} as a concentration rather than a number of molecules and taking N, the number of molecules per volume, to set the strength noise threshold. Our deterministic equations is then of the form

$$\dot{\vec{x}} = \vec{f}(s, \vec{x}) - \vec{g}(\vec{x})$$

and the associated iterative Langevin equation for each component is

$$x_i(t+\tau) = x_i(t) + \tau(f_i(s,\vec{x}) - g_i(\vec{x})) + \sqrt{\frac{\tau}{N}} \left(\sqrt{f_i(s,\vec{x})} \tilde{\Gamma}_i 1(0,1) + \sqrt{g_i(\vec{x})} \tilde{\Gamma}_i 2(0,1) \right)$$
(3.11)

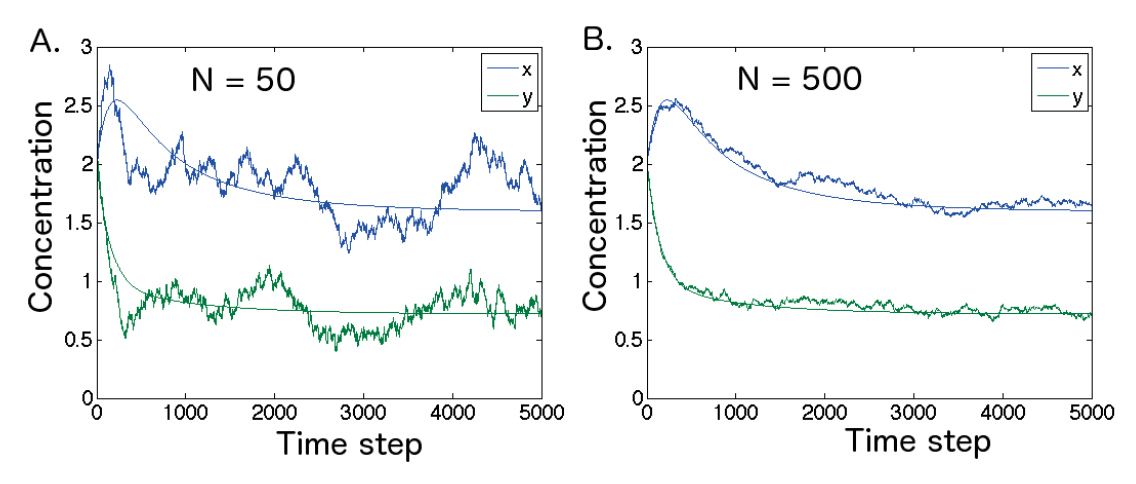


Figure 3–6: Two Langevin realizations for the biological switch, Eq. 3.7 with a=0.45, b=1. A. N=50 leads to big fluctuations. B. N=500 leads to smaller fluctuations.

As an example, we take again the biological switch, Eq. 3.7 and integrate it for N=50 and N=500. Eq. 3.12 is the associated Langevin equation and Fig. 3–6 compares the deterministic solution to the stochastic realization. Note that as N increases, the stochastic result converges to the deterministic curve as expected since in the limit $N \to \infty$, Eq. 3.12 becomes the deterministic equation 3.7.

$$x(t+\tau) = x(t) + \tau \left(y(t) - ax(t)\right) + \sqrt{\frac{\tau}{N}} \left(\sqrt{y(t)}\,\tilde{\Gamma}_{11}(0,1) + \sqrt{ax(t)}\,\tilde{\Gamma}_{12}(0,1)\right)$$
$$y(t+\tau) = y(t) + \tau \left(\frac{x^2(t)}{1+x^2(t)} - by(t)\right) + \sqrt{\frac{\tau}{N}} \left(\sqrt{\frac{x^2(t)}{1+x^2(t)}}\,\tilde{\Gamma}_{21}(0,1) + \sqrt{by(t)}\,\tilde{\Gamma}_{22}(0,1)\right)$$
(3.12)

Chapter 4 - Results

In section 2.3, we introduced the GRN used by Balaskas et. al. [14,17] to model the dependence on the duration of Shh signaling neural tube patterning. According to their model, more ventral neural progenitor identities require longer durations of Shh signaling. We aim to explain their finding and generalize it to higher numbers of genes. We start by simplifying the model to reduce its dimensionality, thereby allowing us to visualize its phase space.

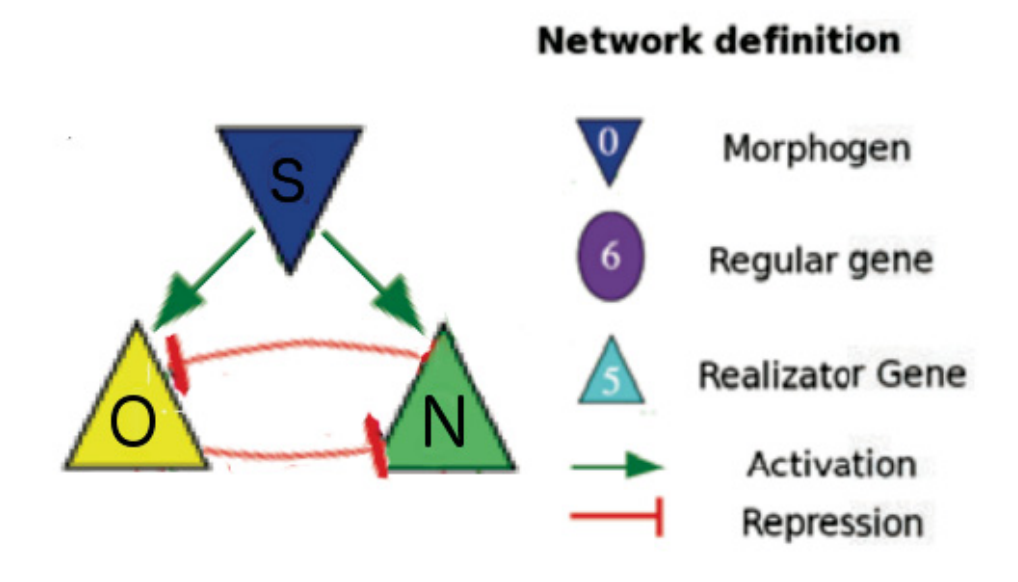


Figure 4–1: Simplified network through the removal of P. The interactions between O, N and S are the same.

In the GRN, Pax6 (P) is an initial state which gets repressed over time by Olig2 (O) and Nkx2.2 (N). Removing P from the network changes the timescale, but does not influence the dynamics we are interested in: O is activated first and N takes over after. We will, therefore, remove and ignore P for the purposes of our analysis, the remaining network is then two dimensional and depicted in Fig. 4–1. Eq. 4.1 with parameters given in Table. 4–1 dictates the possible fates, where we have adopted the convention and notation from Sec. 3.1.

$$\dot{N} = \alpha_N \frac{S^{h_{NS}}}{S^{h_{NS}} + T_{NS}^{h_{NS}}} \frac{T_{NO}^{h_{NO}}}{O^{h_{NO}} + T_{NO}^{h_{NO}}} - \gamma_n N
\dot{O} = \alpha_O \frac{S^{h_{OS}}}{S^{h_{OS}} + T_{OS}^{h_{OS}}} \frac{T_{ON}^{h_{ON}}}{N^{h_{ON}} + T_{ON}^{h_{ON}}} - \gamma_o O$$
(4.1)

Rates					
	N	O			
Production α	5	5			
Degradation γ	1	1			

Hill Coefficients h_{ij} and T_{iS}						
	N O S					
N	0	1	1			
0	5	0	1			

Treshholds T_{ij} and T_{iS}						
N O S						
N	0	1	-1			
О	1	0	-1			

Table 4–1: Table for the simplified 2-dimensional GRN of Fig. 4–1.

4.1 Setup for embryo

Our goal is to make use of a dynamic morphogen signal to create a patterned embryo along an axis. We use this section to present our setup for the *in silico* simulation of an embryo. We define the embryo as an array of cells that can be one, two or three dimensional. We will initially work with a one dimensional embryo where each cell is arranged in a line. Later after having established our result, we will generalize our set up to a two dimensional array of cells where the increased number of neighbors can improve the noise robustness through cell-to-cell interactions.

Consider a GRN such as the one represented by Eq. 4.1. It is a cell autonomous model because it is completely independent of the state of the other cells. Consider now a one dimensional cell array along a position axis. To each cell corresponds a position and we wish to obtain a pattern whereby the array can be separated in two distinct and continuous domains of gene expression. Given the same morphogen input each cell must stabilize in

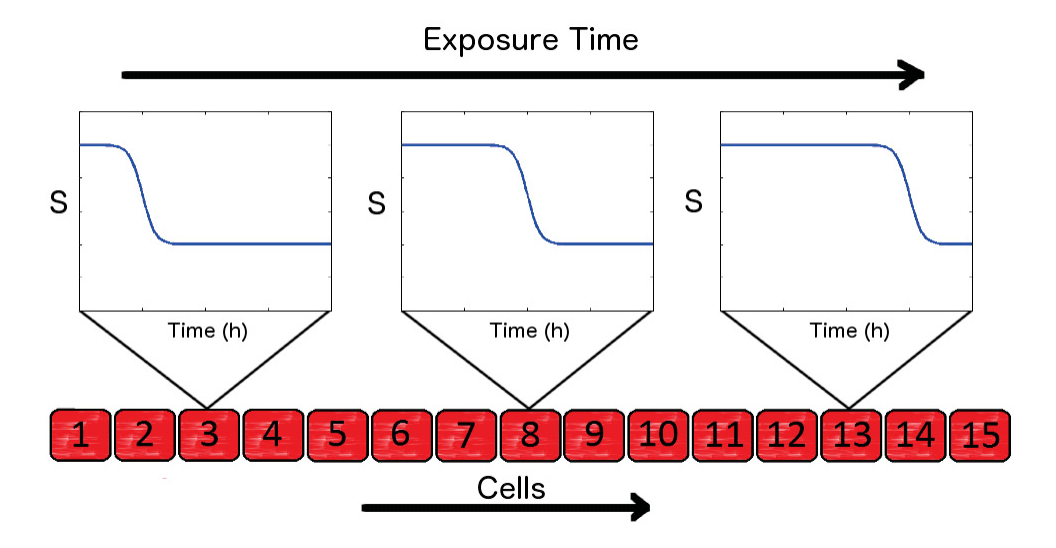


Figure 4–2: We model S as a travelling wave along the embryo. The first cells are exposed for a very brief times and cells farther along the axis are exposed for longer periods of time.

the same fate and as such it is impossible to obtain patterning. The classical solution is to assume the morphogen gradient carries positional information, that is each cell is exposed to a different morphogen concentration as a function of its position. We seek to find a solution to this patterning problem where the concentration is not a function of position. Rather, we seek to expose cells to a constant concentration of morphogen for a given length of time. If each cell is exposed to the morphogen for a different length of time, then positional information can be inferred from exposure time to obtain a Temporal French Flag model.

To vary exposure time, we model Shh as a traveling wave along the embryo. Cells C_m are initially all exposed to the same concentration of morphogen, but after some time the concentration in posterior cells drops to a lower level L, the wavefront due to the drop in concentration travels along the embryo such that progressively more anterior cells are exposed for longer periods of time. After a certain time, Shh reaches steady-state in all cells and cell fate is established. Fig. 4–2 shows Shh as a function of time at various cell positions.

Biologically, cells could acquire different exposure times by leaving a budding region, the longer cells stay in the budding region, the longer they are exposed to the morphogen [23]. Anterior cells are the first to leave the budding region and are therefore exposed for short times. Another way to obtain such a traveling wave is to imagine that S is repressed by another molecule M and that M is absent in the embryo. If the anterior region suddenly

starts producing molecule M, the concentration of S will fall to lower levels L as a result of the repression by M. Over time these molecules M will diffuse through the embryo and posterior cells by their greater distance to the anterior source of M will maintain higher levels of S for a longer period of time. All in all, we make no claim as to why S(t) is a travelling wave along the embryo. We simply model it as such to simulate a Temporal French Flag model.

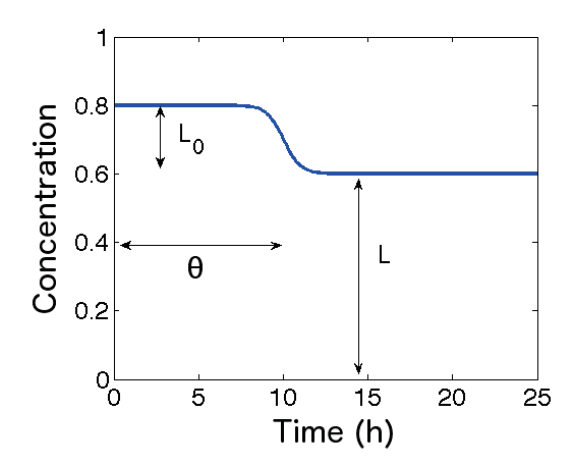


Figure 4–3: We model S as a constant plus a Hill function such that after roughly θ hours, S has fallen to a steady-state concentration.

To model this traveling wave, we take $S_m(t)$ as in Fig. 4–3. The concentration of S at Cell m is a constant L added to Hill function with a threshold θ_m which corresponds to the time of exposure for cell m (Fig 4–2). $L + L_t$ is the initial concentration of S which drops to the steady-state value L after $\approx \theta_m$ time. η , the Hill coefficient quantifies the abruptness of the concentration drop. Eq. 4.2 is the complete mathematical description of the system where $C_m[O], C_m[N], S_m(t)$ is the concentration of O, N, S in Cell m respectively as in Fig. 4–2.

$$S_{m}(t) = L + L_{t} \frac{\theta_{m}^{\eta}}{\theta_{m}^{\eta} + t^{\eta}}$$

$$\dot{C}_{m}[O] = \alpha_{O} \frac{S_{m}^{h_{OS}}}{S_{m}^{h_{OS}} + T_{OS}^{h_{OS}}} \frac{T_{ON}^{h_{ON}}}{C_{m}[N]^{h_{ON}} + T_{ON}^{h_{ON}}} - \gamma_{o}C_{m}[O]$$

$$\dot{C}_{m}[N] = \alpha_{N} \frac{S_{m}^{h_{NS}}}{S_{m}^{h_{NS}} + T_{NS}^{h_{NS}}} \frac{T_{NO}^{h_{NO}}}{C_{m}[O]^{h_{NO}} + T_{NO}^{h_{NO}}} - \gamma_{n}C_{m}[N]$$

$$(4.2)$$

Figure 4–4. shows the solution to Eq. 4.2 for two different values of θ . For both cells, the initial time course is identical, a difference only arises near θ . For the anterior cells, the concentration of S abruptly falls and the system stabilizes in a stable O-state. In posterior cell, while O was initially expressed, it slowly degrades as N takes over. By the time the concentration of S drops in the posterior cell, N is fully expressed and the system simply stabilizes in the N-state. This creates a patterned embryo where anterior cells begin to express O and posterior cells express N. See Fig. 4–5.

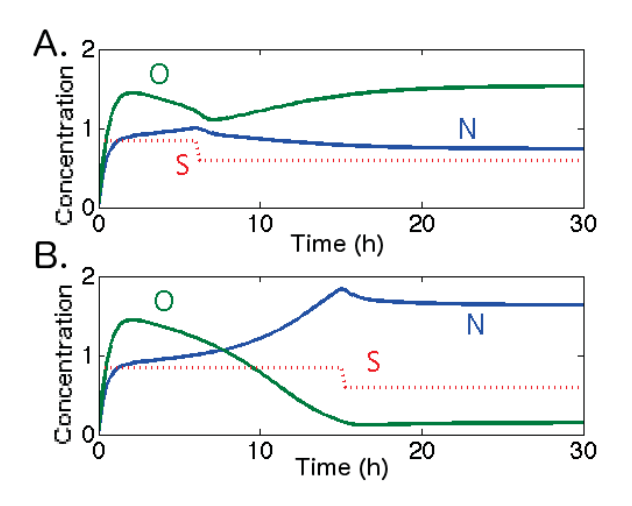


Figure 4–4: Graph of O, N as a function of time for two different exposure times θ . A. $\theta = 7$ B. $\theta = 15$. In both cases O is expressed first, if the system is exposed to S = 0.8 for a sufficiently long time, N is the steady state.

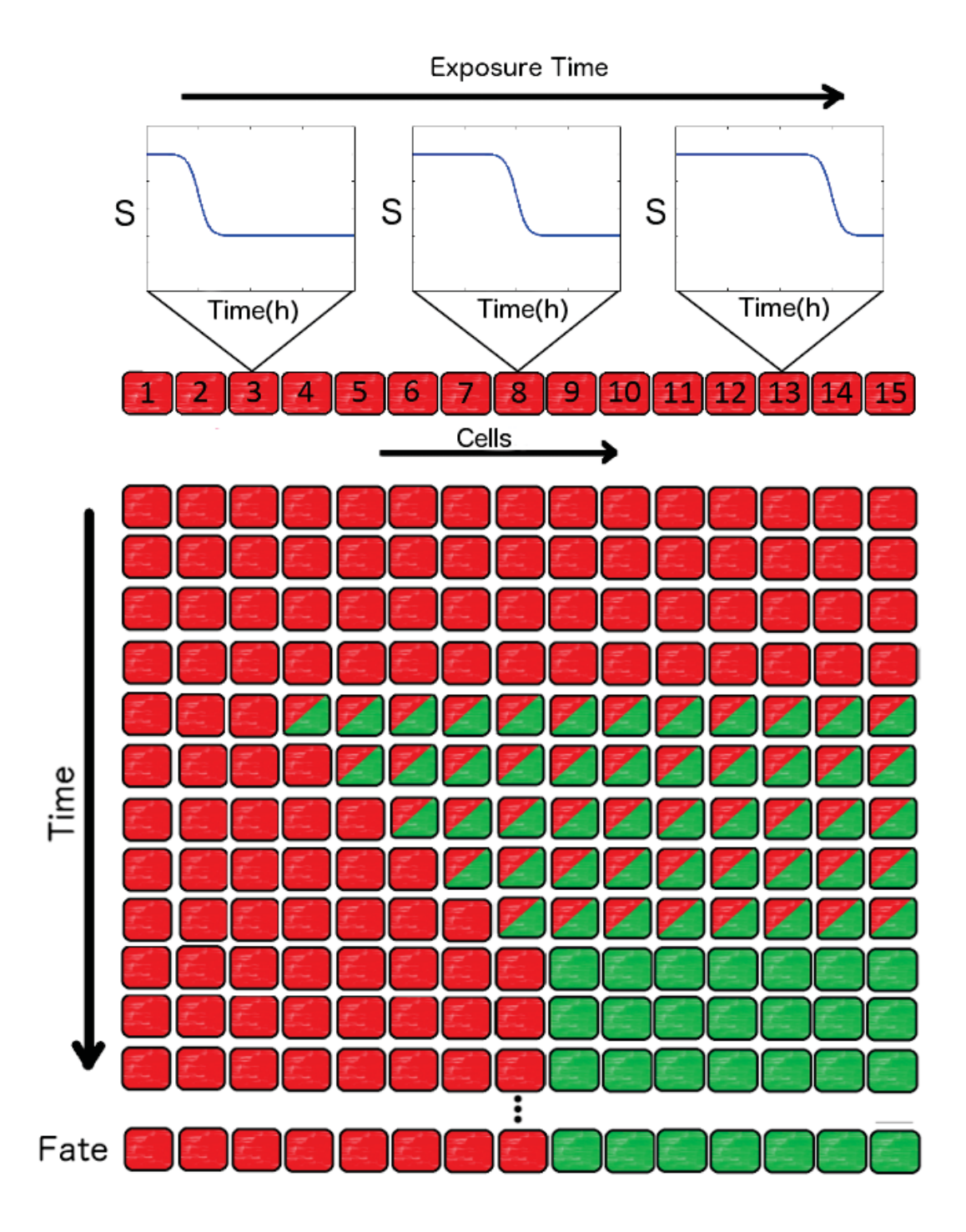


Figure 4–5: We model S as a traveling wave along the embryo. Leftmost cells are exposed for very brief times and cells farther along the axis are exposed for longer periods of time. All cells initially express the same profile (Fig. 4–4), but as they begin to stabilize after θ_m time a 2D pattern is created. Red is high O, Red/Green is a transient state and Green is high N.

4.2 Phase space

Armed with eq. 4.2 we can now evaluate the response of the network to the morphogen Shh (S). Fig. 4–6 shows the phase space for S=0.6. We notice the nullclines cross in three points. Two of them are stable fixed points, they correspond to the N fate and the O fate. In between them there is an unstable fixed point. For initial conditions near the origin, the system is driven to the O fixed point. The separatrix is the line separating the two basins of attraction, the flow cannot cross it and therefore the N state cannot be reached.

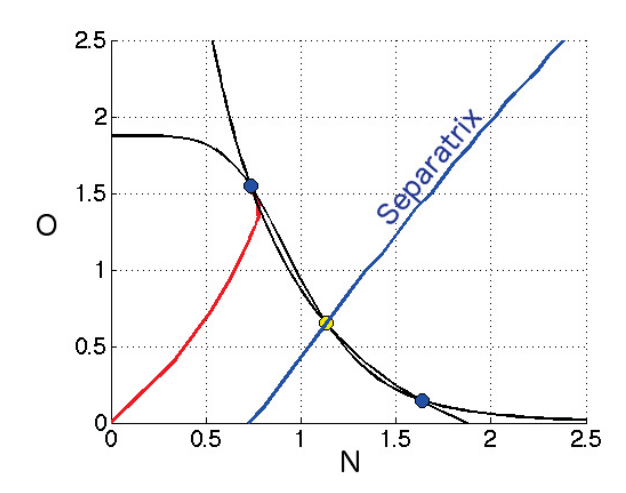


Figure 4–6: Phase portrait of the simplified network 4–1 at S=0.6. The black lines are the nullclines crossing in three points (blue and yellow for stable and unstable respectively). The blue separatrix separates the two domains. The red line is the flow from the origin converging to the O-state.

For larger values of S, the nullclines move and the number of crossings change. Fig. 4–7A. shows the separatrix and fixed points for increasing values of S. The unstable fixed point migrates toward the stable O state and a saddle-node bifurcation happens at $S_+ \approx 0.710$. Fig. 4–7 B. shows the phase space for $S_- = S_+$, the nullclines are near parallel at the bifurcation, the O state having vanished, the flow is free to proceed towards the N state, constrained between the nullclines. Fig. 4–8 is the bifurcation diagram for the process. As S varies from 0 to 1 the position of the fixed points change and two saddle-node bifurcations happen. One at S_+ and another one for lower values at $S_- \approx 0.558$. In the S_- bifurcation, it is the N state that collides with the unstable state, leaving behind the lone O state. Interestingly, this leads to hysteresis which has also been observed in other biological contexts [61].

If we take a look at the gene expression as a function of time we see that N can only be expressed after O recedes. The network spends a long time in the O state before reaching

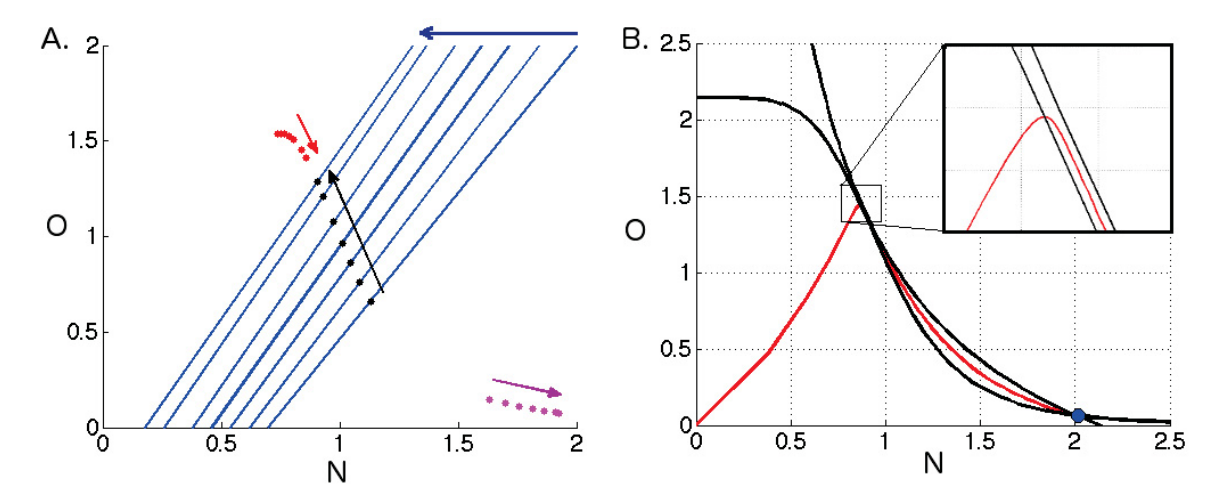


Figure 4–7: Phase portrait of the simplified network 4–1 as a function of S and for $S_+ = 0.710$. A. The red stable O-state moves toward the unstable black point to ultimately annihilate at $S_+ = 0.710$. The blue separatrix moves to the left and the purple stable N-state moves to the right. B. At $S_+ = 0.710$, the nullclines are nearly parallel and the flow is constrained to move between the nullclines until it reaches steady-state at the N-state.

the N state, on the order of 12 hours. This is relatively slow and not comparable to the typical degradation rate $(\gamma_o, \gamma_n = 1)$. Not only that, but the typical time before activation of N is variable and controlled by S. Fig. 4–9 shows the time series for decreasing values of S, O persists for longer and longer until $S = S_+$ leads to stabilization. The timescale becomes infinite when $S \to S_+$ from above.

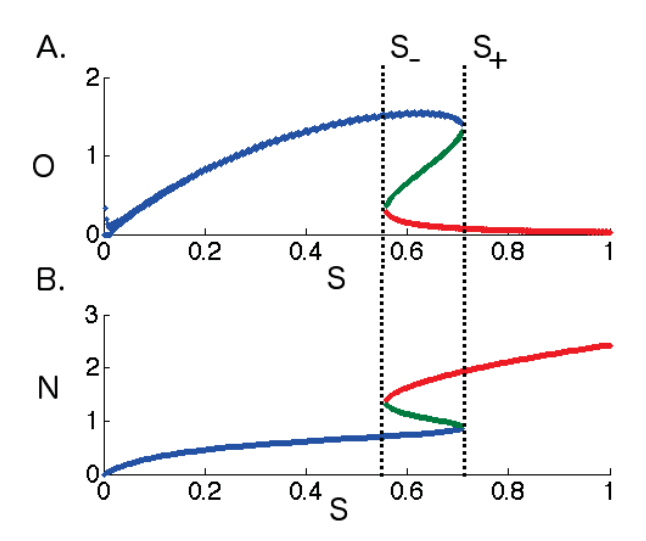


Figure 4–8: Bifurcation diagram simplified network 4–1 as a function of S. Two saddle-node bifurcations happen. The first one at $S_{-}=0.558$ leads to the creation of the N state and an unstable fixed point. The unstable fixed point then migrates towards the O-state and collides with it during the second saddle-node bifurcation at $S_{+}=0.710$ A. Concentration of O of the fixed points as a function of S. B. Concentration of S. Oncentration of S.

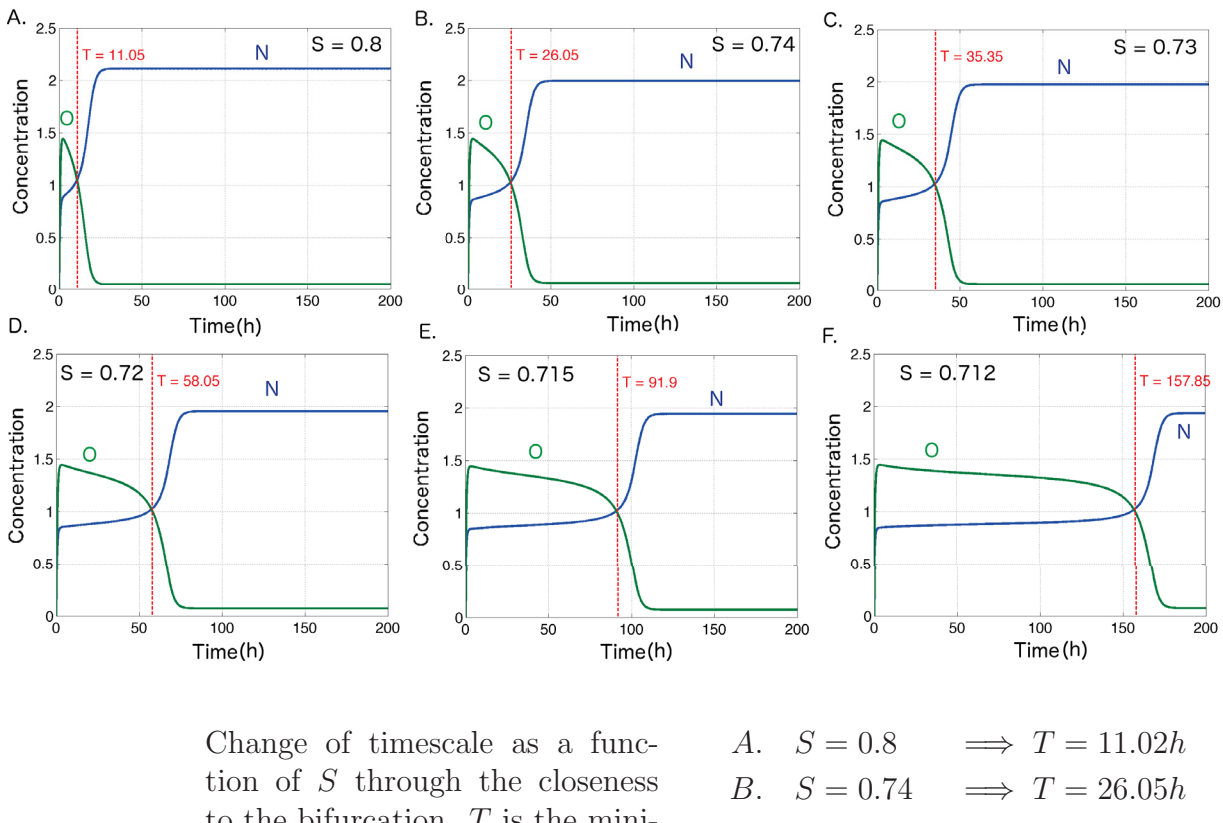


Figure 4–9: to the bifurcation. T is the minimum time of exposure needed to converge to the N-state. As Sapproaches S_+ from above, the timescale becomes infinite.

$$C. \quad S = 0.73 \quad \Longrightarrow T = 35.35h$$

$$D. \quad S = 0.72 \quad \implies T = 58.05h$$

$$E. \quad S = 0.715 \quad \Longrightarrow \quad T = 91.9h$$

$$F. \quad S = 0.712 \quad \Longrightarrow \quad T = 157.85h$$

This slow timescale persist in phase space, an attractive line exists between the nullclines where motion along the curve is much slower than motion transverse to it. Effectively, the flow converges quickly on the line and then slowly relaxes to the fixed point N. We will term this curve the "Valley" and analyze it from the point of view of slow manifold theory.

4.3 Analytical Solution

We write eq. 4.1 in a more compact form and use parameters as chosen by Balaskas [14]. We will proceed to locally analyze the phase space. We Taylor expand near an arbitrary point $(N_0, O_0) = \vec{x}_0$ to get the linear ODEs, Eq. 4.3 where f, g are Hill functions.

$$\dot{N} = f(O) - N \approx f'(O_0)O - N + f(O_0) - f'(O_0)O_o
\dot{O} = q(N) - O \approx q'(N_0)N - O + q(N_0) - q'(N_0)N_o
\equiv \dot{\vec{x}} = \hat{A}(x_o)\vec{x} + \vec{B}(x_0)$$
(4.3)

This is valid only for $\vec{x} = \begin{pmatrix} N \\ O \end{pmatrix}$ near \vec{x}_o . The matrix \hat{A} and vector \vec{B} depend on $\vec{x_0}$ but are otherwise constant once we have chosen a specific point \vec{x}_0 we are interested in. The eigenvalues λ_{\pm} and eigenvectors \vec{v}_{\pm} of \hat{A} can be computed and are relevant to define the slow manifold.

$$\lambda_{\pm} = -1 \pm \sqrt{g'(N_0)f'(O_0)}, \quad \vec{v}_{\pm} = \begin{pmatrix} \pm \sqrt{\frac{f'(O_0)}{g'(N_0)}} \\ 1 \end{pmatrix}$$
 (4.4)

Fixed points correspond to points \vec{x}_0^* such that $\dot{\vec{x}} = \hat{A}\vec{x}_0^* + \vec{B} = 0$. At a fixed point \vec{x}_0^* , we read the stability along \vec{v}_{\pm} from the sign of λ_{\pm} . When $S < S_+$, there are three fixed points, which we label \vec{x}_O^* , \vec{x}_N^* , \vec{x}_U^* for the O state, the N state and the unstable state respectively. At $S = S_+$, $\vec{x}_O^* = \vec{x}_U^*$ as the two fixed points collide, we call \vec{x}_C^* the critical point where the O state meets the unstable state. The collision implies implies that $\lambda_{O,\pm} = \lambda_{U,\pm}$ at $S = S_+$. For $S < S_+$ we have $\lambda_{O,\pm} < 0$ by stability of O and $\lambda_{U,+} > 0$, $\lambda_{U,-} < 0$ because \vec{x}_U^* is a saddle. By continuity, this forces $\lambda_{U,+} = \lambda_{O,+} = 0$ when $S = S_+$. This means that $\vec{v}_{C,+} = \vec{v}_{O,+} = \vec{v}_{U,+}$ defines a slow manifold at \vec{x}_C .

To see how a slow manifold would arise near a region with a large separation in eigenvalues, consider a linear system like in eq. 4.3 near a point \vec{x}_0 such that $|\lambda_+| \ll |\lambda_-|$. The solution is then

$$\vec{x} = ae^{\lambda_{+}t}\vec{v}_{+} + be^{\lambda_{-}t}\vec{v}_{-} - \hat{A}^{-1}\vec{B}$$
(4.5)

with a and b are given by initial conditions, i.e. a, b such that $\hat{A}\vec{x}_{t=0} + \vec{B} = a\vec{v}_+ + b\vec{v}_+$. In the case of $|\lambda_+| \ll |\lambda_-|$, $be^{\lambda_-t}\vec{v}_-$ goes to zero much faster than $ae^{\lambda_+t}\vec{v}_+$ as in Fig. 4–10 and the motion lies parallel to \vec{v}_+ . Therefore the dynamics is quickly canalized on a 1D manifold defined by v_+ at the bifurcation.

To find an equation for this 1D manifold, we make explicit use of the constraints that the flow is parallel to \vec{v}_+ . In the case of first order ODEs, such as the one we are dealing with, the flow is entirely constrained by $\dot{\vec{x}}$, therefore the constraint we are looking for is $\dot{\vec{x}} \propto \vec{v}_+$. This is a local statement, at a given point \vec{x}_0 , we are computing the eigenvector of $\hat{A}(\vec{x}_0)$ from the linearization at \vec{x}_0 and comparing it to the flow $\dot{\vec{x}}$ at \vec{x}_0 . We take the set of

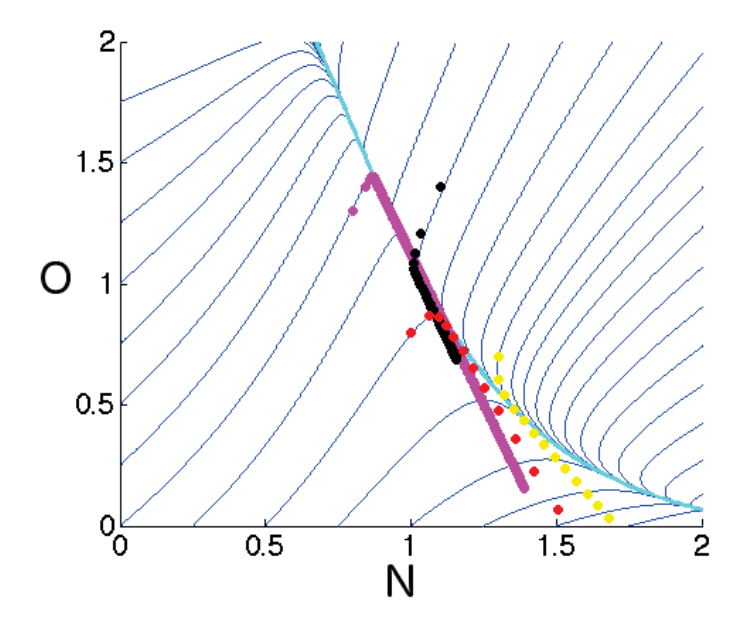


Figure 4–10: Linear solution of Eq. 4.3 for various initial conditions. The colored dots are the linear solution plotted with a constant time step of 30 min, it illustrates a quick convergence onto a slowly moving line. The thin blue lines represent the flow in phase space and the thick cyan line is the "Valley".

all points $\{\vec{x}_0 \text{ s.t. } \dot{\vec{x}}(\vec{x}_0) \propto \vec{v}_+(\vec{x}_0)\}$ for which this condition holds to be the slow manifold. In actuality, the equation $\dot{\vec{x}} = \vec{v}_+$ is only approximate, it becomes exact at the critical point \vec{x}_C^* and when $S = S_+$, elsewhere it is only approximate because the linear term in the Taylor approximation is non-zero. When $S < S_+$, the equation is also approximate because we are not at a fixed point and because λ_+ is not identical to zero. As long as $\lambda_+ \approx 0$ and the linear term in the Taylor expansion is small, the equation will be approximately valid.

We now apply the constraint $\dot{\vec{x}} \propto \vec{v}_+$ to the system at hand.

$$\dot{\vec{x}} = \begin{pmatrix} \dot{N} \\ \dot{O} \end{pmatrix} = \begin{pmatrix} f(O) - N \\ g(N) - O \end{pmatrix} \propto \begin{pmatrix} \pm \sqrt{\frac{f'(O)}{g'(N)}} \\ 1 \end{pmatrix} = \vec{v}_{+}$$
 (4.6)

Eq. 4.6 is a system of three unknowns, N, O and α the constant of proportionality between $\dot{\vec{x}}$ and \vec{v}_+ , and two equations corresponding to the two dimensions of the vectors. Solving this system of equations, we obtain Eq. 4.7, the implicit equation between N and O describing the valley. Fig. 4–11 shows the implicit curve along with linear solutions converging to the valley.

$$(f(O) - N) = (g(N) - O)\sqrt{\frac{f'(O)}{g'(N)}}$$
(4.7)

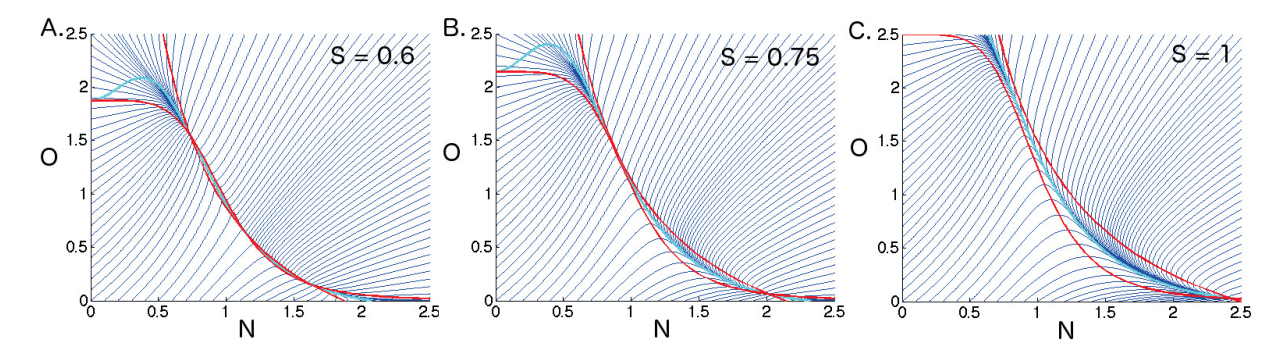


Figure 4–11: Implicit plot of the Valley for different values of S. Blue lines are the flow and the cyan curve is the valley as given by Eq. 4.7 Red are the nullclines. A. S=0.6 the valley is tightly snug between the nullclines. B. S=0.75, just past the bifurcation, Eq. 4.7 approximates the canalization of the flow very well. C. S=1, well past the bifurcation the nullclines start to separate and the difference between the flow and Eq. 4.7 becomes visible.

Finally, we can take the norm of $\dot{\vec{x}}$ to find the phase space "velocity" along the valley. This is in a sense how quickly gene concentration changes as a function of time. Fig. 4–12 A. compares the true velocity and eq. 4.8 as a function of time for a trajectory starting from the origin. The agreement is optimal near the critical point. Fig. 4–12 B. shows the eigenvalues as a function of time for the same trajectory, λ_+ is closest to zero when the velocity is slowest.

$$v = \|\dot{\vec{x_v}}\| = |g(N_v) - O_v| \|\vec{v_+}\| = |g(N_v) - O_v| \sqrt{1 + \frac{f'(O_v)}{g'(N_v)}}$$
(4.8)

Expression 4.8 is also helpful to understand the origin of the slow time-scales: near the critical point $v \propto |g(N_v) - O_v| \approx 0$ as it is the O component of $A\vec{x}_0 + \vec{B}$ so the system will escape the ghost fixed point in a time $\tau \propto \frac{1}{v}$, which is big compared to any parameter of the system. This explains the "timing effect": much of the time evolution of the system is spent close to the O ghost state. This becomes especially noticeable very close to the bifurcation as $\tau \to \infty$. It is important to note that the approximation breaks down as we get further from the bifurcation and the distance between the nullclines increases which indicates that $A\vec{x}_0 + \vec{B}$ becomes big.

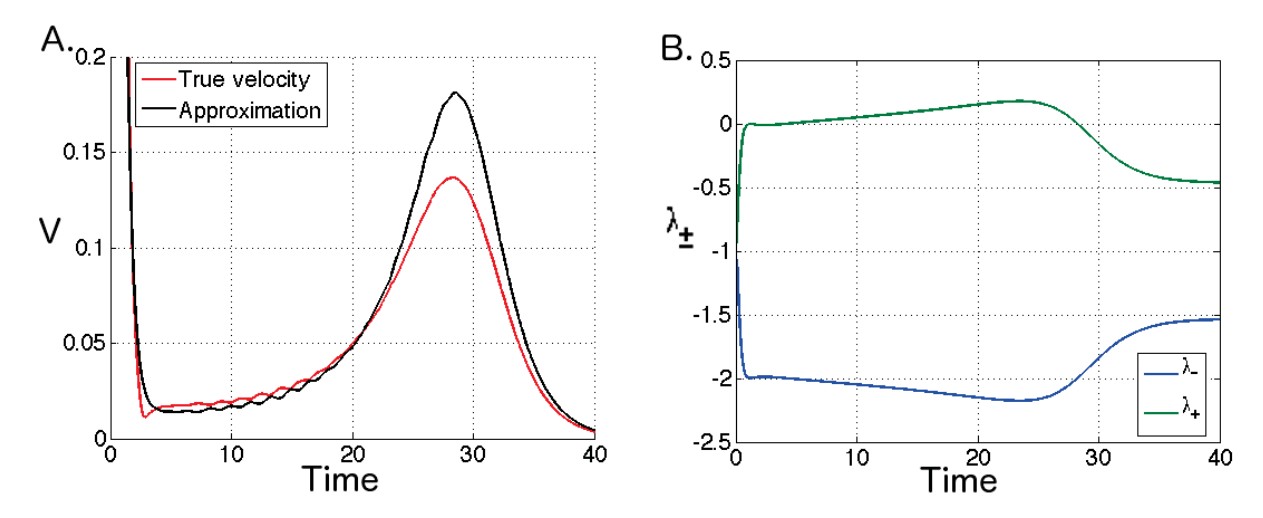


Figure 4–12: Comparison of phase space velocity, the approximate Valley velocity and the eigenvalues as a function of time. A. The true velocity as a function of time of a trajectory starting from the origin is well approximated by Eq. 4.8 when the nullclines are close. B. The eigenvalues of \hat{A} are plotted as a function of time for a trajectory starting from the origin. λ_+ is very near zero once the flow canalizes on the valley.

4.4 Higher dimension

Having elucidated the mechanism by which patterning emerges in the presence of a temporal gradient of Sonic Hedgehog, we seek to generalize our results to higher dimensional gene networks. We search for a gene network template that is easily altered to produce networks leading to as many domains as genes (that is, we only want realizator genes). We also want to preserve the scaling property of the domains as well as the sequential expression of the genes as a function of time. Fig. 4–13 shows the concentration of a morphogen M as a function of time with the corresponding desired temporal gene expression leading to a clearly defined pattern.

To make clear the fact that only the transient behaviour of the morphogen is needed for patterning, we choose L, the steady-state concentration of M to be equal to zero, (Fig. 4–14. In order for the gene expression to be sustained when no (activating) morphogen is present it is necessary to either have self-activation or make M a repressor. We choose the latter option and in addition require that our gene networks be fully repressing, that is, each gene represses every other gene albeit with varying strength. This choice is also motivated by recent findings which have shown that mutual repression enhances the steepness and precision of gene expression boundaries [54]. The ODEs corresponding to the set up with

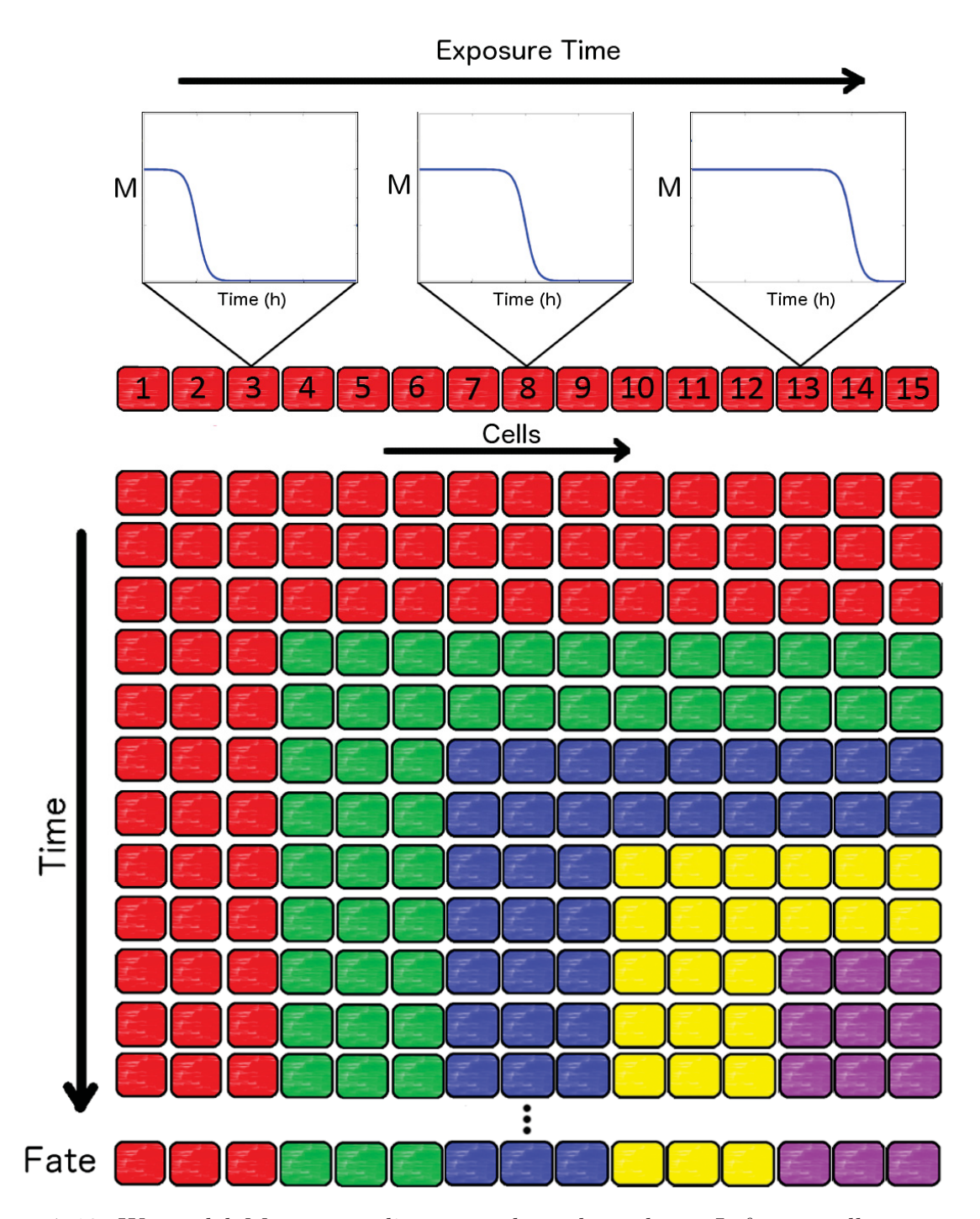


Figure 4–13: We model M as a traveling wave along the embryo. Leftmost cells are exposed for very brief times and cells farther along the axis are exposed for longer periods of time. All cells initially express the same profile, but as they begin to stabilize after θ_m time the profile of later cells diverges and explores new states. Each color corresponds to a gene G_i expressed in the same temporal order as their positional order.

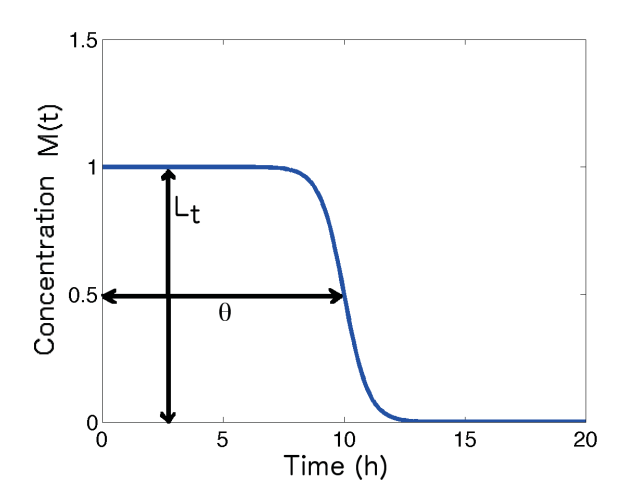


Figure 4–14: We model M as a Hill function such that after roughly θ hours, M has fallen to a steady-state concentration of 0.

parameters in Table 4–2 is summarized in Eq. 4.9 in accordance to our notation from Sec. 3.1 with the difference that the lack of activating genes has been made explicit and we assume a single repressing morphogen M.

$$M(t) = L_t \frac{\theta^{\eta}}{\theta^{\eta} + t^{\eta}}$$

$$\frac{dG_i}{dt} = \alpha_i \text{Hill}(M, T_{iM}, h_{iM}) \prod_{h_{ij} \le 0} \text{Hill}(G_j, T_{ij}, h_{ij}) - \lambda_i G_i$$

$$(4.9)$$

The pattern of interactions for the n genes is clear, G_i represses all genes strongly except its successor G_{i+1} which it represses at a higher threshold. Fig. 4–15 recapitulates this pattern, only the weak repressions are shown together with the interaction of the morphogen. Not shown are the arrows of strong repression between all genes except their successor. By keeping the same pattern while increasing the number of genes, we can generate gene networks that give rise to an arbitrary number of domains equal to the number of genes.

This choice of parameters essentially builds ordered interactions that direct the flow in phase space from one gene to its successor, as shown in Fig. 4–16 A. When S is high, genes repress each other in such a way that when G_i is expressed, only G_{i+1} can be produced. As G_{i+1} accumulates, it starts to repress G_i . After some time G_{i+1} wins over G_i and the cycle continues with the accumulation of G_{i+2} . This stops when i = n where the specific parameter T_{1n} has been chosen so that G_1 the successor of G_n cannot be produced. When S is low, genes repress each other in such a way that only one gene can be expressed. The n steady-states then correspond to high concentration of the n genes.

Rates						
$ G_1 G_2 G_3 G_4 G_5$						
Production α	6	6	6	6	6	
Degradation γ	1	1	1	1	1	

Hill Coefficients h_{ij} and T_{iM}						
	G_1	G_2	G_3	G_4	G_5	M
G_1	0	5	5	5	5	3
G_2	5	0	5	5	5	3
G_3	5	5	0	5	5	3
G_4	5	5	5	0	5	3
G_5	5	5	5	5	0	3

Treshholds T_{ij} and T_{iM}							
	G_1	G_2	G_3	G_4	G_5	M	
G_1	0	0.4	0.4	0.4	0.4	1.5	
G_2	2.5	0	0.4	0.4	0.4	1.5	
G_3	0.4	2.5	0	0.4	0.4	1.5	
G_4	0.4	0.4	2.5	0	0.4	1.5	
G_5	0.4	0.4	0.4	2.5	0	1.5	

Table 4–2: Table for the n = 5 dimensional GRN of Fig. 4–15.

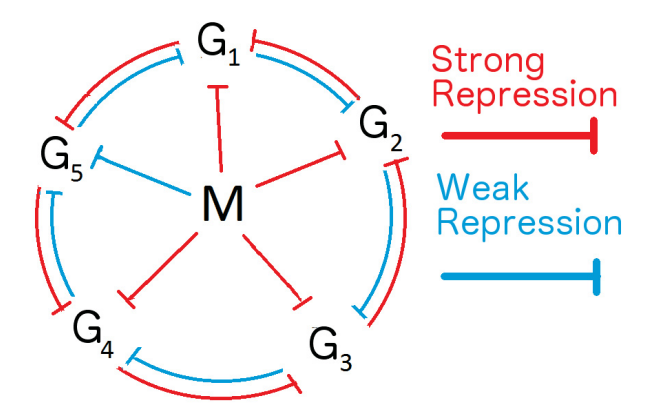


Figure 4–15: 5D generalized GRN. All genes strongly repress each other (not shown), except the neighbor interactions which are shown. Blue and red arrows label weak or strong repression, respectively. M, the morphogen, represses all genes equally except G_5 . Parameters as given in Table 4–2

The structure of the interaction is such that at any given time, only three genes can be expressed, G_{i-1} , G_i , G_{i+1} . The entire flow during such a transition is therefore constrained to a 3D phase space as shown in Fig 4–16 B. The trajectory is similar to the 2D valley we uncovered in Sec. 4.3. In Sec. 4.5, we will see that locally, the two are the same.

Like its two dimensional counter part, there is an emerging time scale which can be varied through a single parameter. Eq. 4.10 defines the effective production rate of gene G_i as a

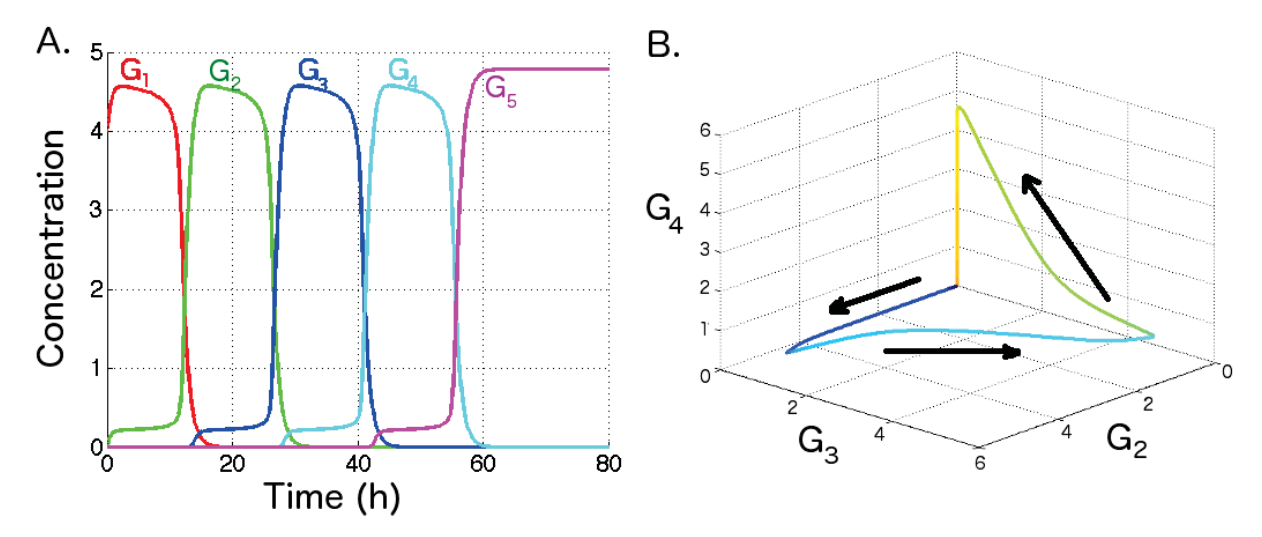


Figure 4–16: Trajectories of the 5D GRN with parameters in Table 4–2, with the exception of $T_{iM} = 1.58$ and associated flow for M = 1. A. G_i versus time. B. 3D phase portrait of G_2, G_3, G_4 , neighboring genes are connected by a valley.

function of the repression due to M. $\alpha_{i,\text{eff}}$ can be varied by changing any of $\alpha_i, M, T_{iM}, h_{iM}$. We will vary T_{iM} specifically because it allows control of expression time for an individual G_i through $\alpha_{i,\text{eff}}$.

$$\alpha_{i,\text{eff}} = \alpha_i \text{Hill}(M, T_{iM}, h_{iM}) \tag{4.10}$$

The duration of expression of a gene G_i gives rise to a domain of proportional length (Fig. 4–17) such that by varying the parameter T_{iM} , which controls the length of time spent expressing G_i , directly influences the length of the domain. Fig. 4–17 shows this principle in action. By changing T_{3M} we induce a very long domain of cells with fate G_3 . Similarly by changing all T_{iM} equally, we can speed up or slow down the entire process which leads to a shortened or elongated pattern. Not surprisingly, if we connect G_5 to G_1 by weakening the repression threshold to $T_{15} = 0.4$ and we get an oscillator resulting in an oscillating pattern as in Fig. 4–17.

4.5 Bifurcation analysis

The many interesting properties due to the criticality still occur and we can approximate the valley following the same methodology as that applied to the 2D valley case in Sec 4.3. As $\alpha_{i,\text{eff}}$ is varied, either by changing M or T_{iM} , there is a critical point for which the system

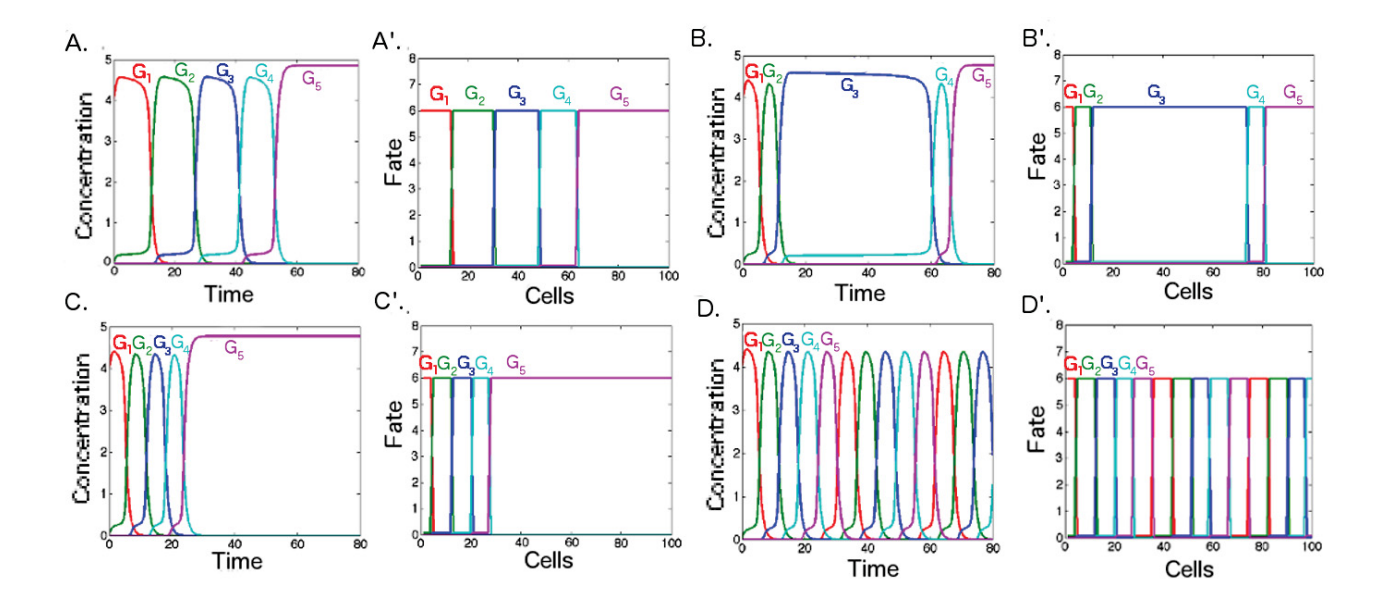


Figure 4–17: A bifurcation controls the timescale of individual genes. By changing T_{iM} we can lengthen or shorten the timescale of individual genes which leads to scaled domains. All figures are the timescales of G_i for M=1. A. A'. shows $T_{iM}=1.58$ which leads to a slow timescale for the whole embryo. B. B'. $T_{iM}=1.5$, $T_{3M}=1.575$ leads to a long timescale for G_3 . C. C'. $T_{iM}=1.5$ for all genes leads to a very fast timescale and short domains. D. D'. By connecting G_5 to G_1 through $T_{51}=0.4$ we get an oscillator that stabilizes into oscillating domains.

undergoes a local saddle-node bifurcation which creates a stable fixed point for the gene G_i . This bifurcation is the very reason why T_{iM} can be varied to change the domain lengths. To study this network, we proceed to linearize the system at an arbitrary point \vec{P} in phase space. The entries of \vec{P} are some concentrations P_i corresponding to the *i*th gene.

Because the system is five dimensional, the linearisation of the system is much more complicated, in particular the Jacobian matrix

$$\hat{A}(\vec{P}) = \left. \frac{d\dot{G}_i}{dG_j} \right|_{G_i = P_i}$$

contains many non-zero terms depending on P_i and is hard to visualize. However, near the peaks of maximum gene expression where the bifurcation happens, the matrix \hat{A} simplifies and becomes effectively 2D. In the case of the G_2 peak (the block matrix shifts up or down depending on which peak we linearize at), we have

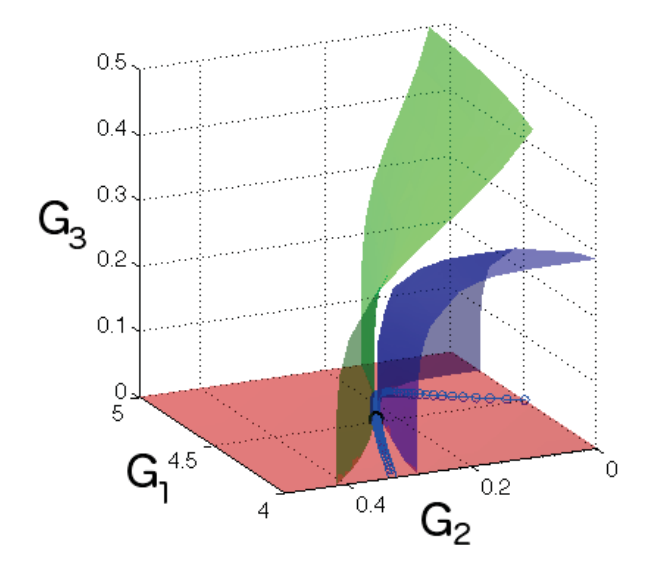


Figure 4–18: The nullclines are hyperplanes whose projection is shown here for G_1, G_2, G_3 at the first peak. $T_{iM} = 1.58, M = 1$. The blue curve is the valley stuck in between the nullclines. Compare with Fig. 4–7

$$\hat{A}(\text{2nd Peak}) = \begin{pmatrix} -1 & 0 & 0 & 0 & 0\\ 0 & -1 & f'(P_3) & 0 & 0\\ 0 & g'(P_2) & -1 & 0 & 0\\ 0 & 0 & 0 & -1 & 0\\ 0 & 0 & 0 & 0 & -1 \end{pmatrix}$$

where f and g are the Hill functions between genes G_2 and G_3 evaluated at $G_2 = P_2$ and $G_3 = P_3$ with their respective parameters. Focusing on the 2x2 block, we have as before the eigenvalues and eigenvectors

$$\lambda_{\pm} = -1 \pm \sqrt{g'(P_2)f'(P_3)}, \quad \vec{v}_{\pm} = \begin{pmatrix} 0 \\ \pm \sqrt{\frac{f'(P_3)}{g'(P_2)}} \\ 1 \\ 0 \\ 0 \end{pmatrix}$$

This exact correspondence allows the computation of the approximate valley near the peaks by removing the fast degrees of freedom and keeping the flow parallel to the slow eigenvector. However, the approximation breaks down as the system departs from the peak. The effect of the other genes becomes non-negligible leading to non-zero terms in the matrix

A which regains its full dimensionality in the trough between peaks. As the system enters another peak, the matrix becomes block diagonal again and the system follows the new slow eigenvector, creating a new valley. In the transition between the peaks, all eigenvalues converge to -1 at the same time, it is therefore impossible to follow an eigenvector from one peak to another, as such the valley can only approximate peaks and cannot be analytically connected at the troughs.

As before, this local behaviour explains the change in timescale as we vary T_{iM} to go closer to a bifurcation: the system spends more time close to a "former-fixed-point" as $\lambda_{+} \approx 0$, which gives rise to a bigger domain of expression at steady state for the corresponding gene as in Fig 4–17.

One can use the relation $\vec{v}_+ \propto \frac{d\vec{G}}{dt}$ to determine an approximate equation for the valley that holds in the vicinity of the bifurcation. It is of the same form as Eq. 4.7. The method consists of solving a system of two equations in three unknowns to find an implicit relationship between G_i and G_{i+1} . Alternatively, one can perform a detailed approach and obtain a system of five equations in six unknowns, but there is little hope of solving such a system.

4.6 Stochastic analysis

Up to now, we have only considered development and patterning as a deterministic process. In reality, the cell environment is very noisy due to the fact that only a finite number of molecules are interacting and the process is inherently stochastic. In Sec 3.5, we presented theory of the chemical Langevin equation which we use to numerically simulate noise using the Tau Leapping algorithm.

To have a useful model, it needs to be robust to noise, or at least we must offer an argument for how it can be made more robust [51]. There is an obvious problem when considering a system that evolves in time stochastically. Time compounds noise, especially in system with sharp transitions such as those we present. The fact that there is a bifurcation with a time scale finely controlled by the proximity to a critical value also means that there is a trade off between noise robustness and the ability to produce domains of variable length.

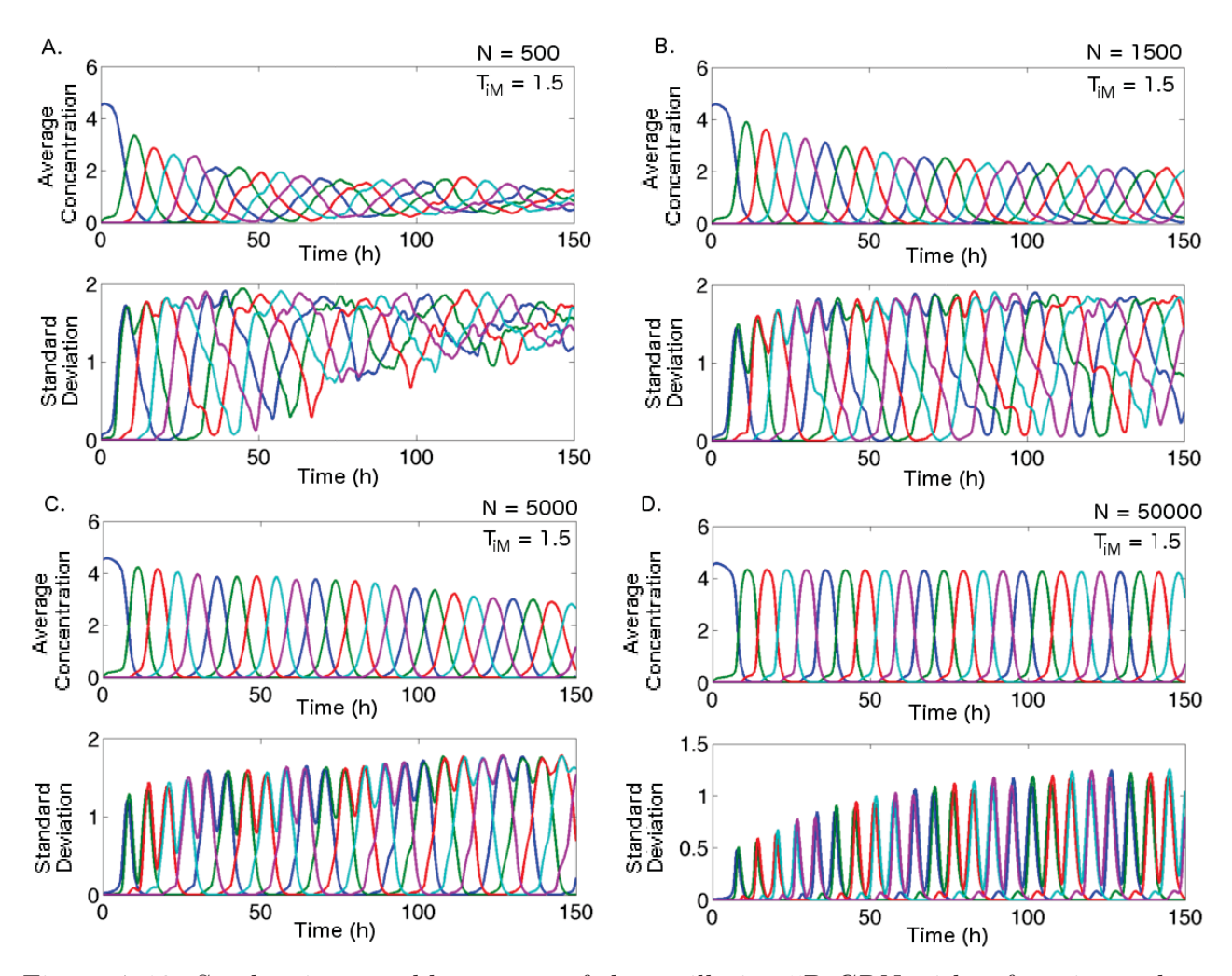


Figure 4–19: Stochastic ensemble average of the oscillating 5D GRN with a fast timescale, $T_{iM} = 1.5$ and different N. The higher N the closer to the deterministic result and the variance becomes constrained to the transition between two genes. For smaller N, the variance increases quickly and the predictive power is lost. A.-D. represent the values of N = 500, 1500, 5000, 50000.

Figure 4–19 and 4–20 show ensemble averages of many trials at a given noise level, controlled by N, the number of molecules in a given volume. The average time course resembles the deterministic time course and in the $N \to \infty$ we retrieve the deterministic solution. However, for smaller N, the peaks' amplitudes of gene expression are decaying as a function of time, as the variance increase. As time goes on, we lose predictive power and it becomes impossible to predict which state will be expressed at some later time t. This actually becomes worse as T_{iM} is adjusted to lengthen the domains. For comparison, the average number of transcription factors for a given gene in a cell lies between 1000 and 5000.

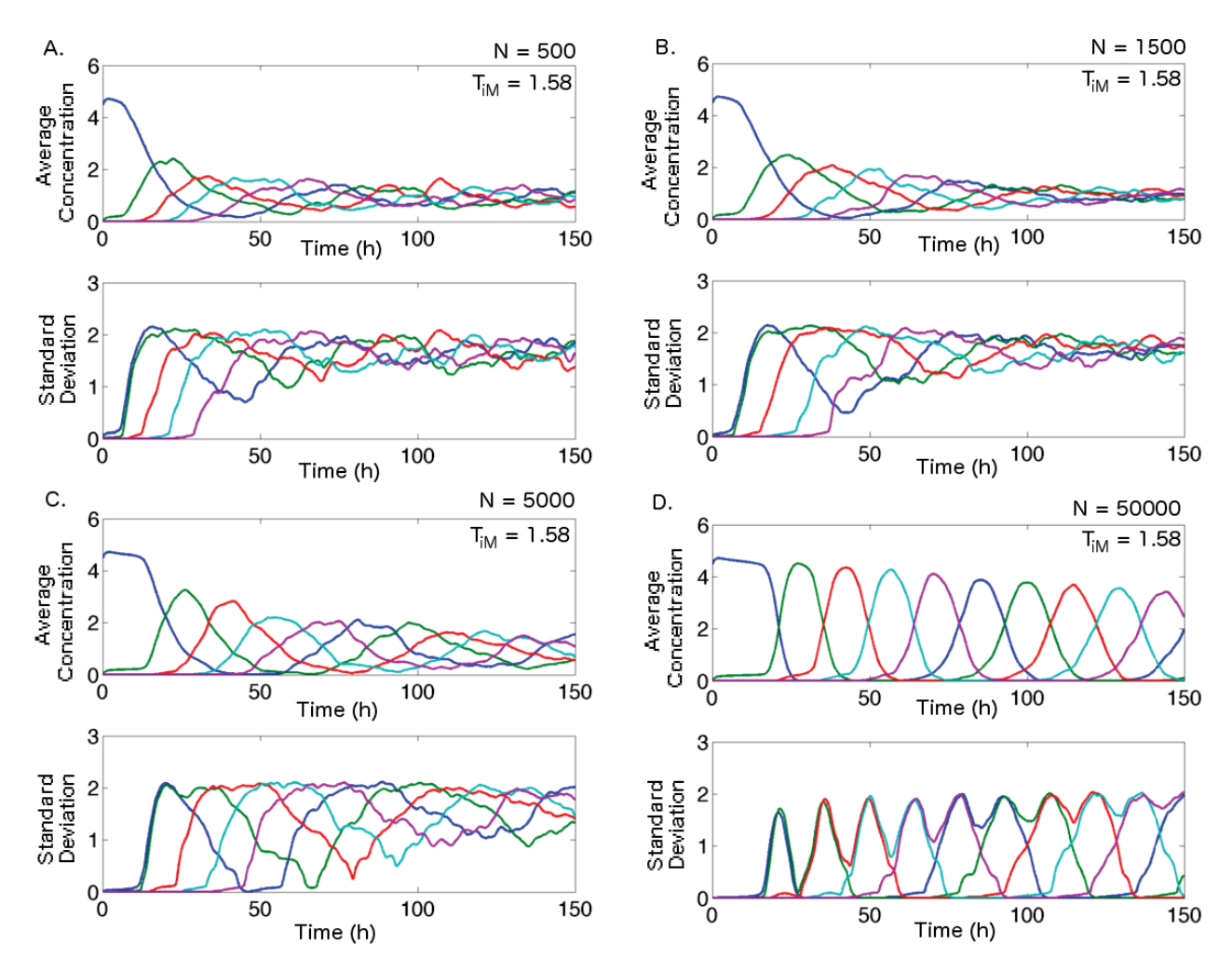


Figure 4–20: Stochastic ensemble average of the oscillating 5D GRN with a slow timescale, $T_{iM} = 1.58$ and different N. The GRN with slow timescale is much more sensitive to the noise than the fast one. The higher N the closer to the deterministic result and the variance becomes constrained to the transition between two genes. For smaller N, the variance increases quickly and the predictive power is lost. A.-D. represent the values of N = 500, 1500, 5000, 50000.

To remedy this problem, we therefore propose a model by which cells interact with each other to reduce noise.

4.6.1 Cell averaging

For this part, we simulate cell development with a two dimensional cell array. Each cell C_{mn} is exposed to a concentration of morphogen M_{mn} as in Sec. 4.1. We model S_{mn} as a travelling wave propagating along the x axis so that each cell along the y axis is exposed to the same concentration of M at a given time.

Cell sorting has been suggested as a way to repair the effect of noise [62]. An alternative is to postulate cell-to-cell interactions. To model cell interactions we will add an interaction term to our set of coupled ODEs. The resulting system is not cell autonomous and requires keeping track of every cell individually. To motivate the form of our interaction term, we note that it is known that cells interact with each other through many means such as simple diffusion, endocytosis, the use of transport proteins such proteoglycans or signaling pathways (e.g. Notch) [63]. Rather than modeling a particular form of cell-to-cell interaction, we want a phenomenological effective term. We model interactions between two cells using the rate function

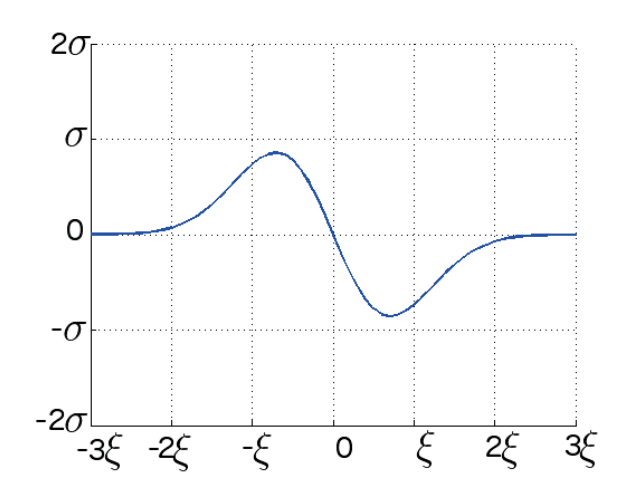


Figure 4–21: Shape of the cell-to-cell interaction function which scales according to ξ_{int} the interaction length and σ_{int} the interaction strength. Given two cells with gene concentrations G and G^* , they interact with a rate $\approx \sigma$ when $|G - G^*| \approx \xi$ towards their average.

$$F_{int}(C_{mn}[G_i] - C_{pq}[G_i], \xi_{int}, \sigma_{int}) = -\frac{\sigma_{int}(C_{mn}[G_i] - C_{pq}[G_i])}{\xi_{int}} e^{-\left(\frac{C_{mn}[G_i] - C_{pq}[G_i]}{\xi_{int}}\right)^2}$$
(4.11)

where $C_{mn}[G_i]$, $C_{pq}[G_i]$ are the concentration of the gene G_i in the two different cells indexed by (m, n), (p, q) in the cell array, ξ_{int} is the length of interaction sets a concentration scale¹ past which the cells do not interact and σ_{int} is the strength of interaction which plays the role of the rate at which the interaction happens.

¹ By interaction length, we do not mean physical distance between cell, but difference between gene concentrations.

The purpose of this interaction is to average the difference between two interacting cells. When $C_{mn}[G_i] - C_{pq}[G_i]$ is zero, the function returns zero and there is no interaction. When $|C_{mn}[G_i] - C_{pq}[G_i]| \gg \xi_{int}$ the cells are deemed dissimilar and they do not interact. If $|C_{mn}[G_i] - C_{pq}[G_i]| \lesssim \xi_{int}$, the cells interact in such a way as to return to their mean. If $C_{mn}[G_i] > C_{pq}[G_i]$, F_{int} will be an effective degradation rate and if $C_{mn}[G_i] < C_{pq}[G_i]$, F_{int} will be an effective production rate. The function F_{int} is plotted in Fig. 4–21. it has the shape of the first excited state of the quantum harmonic oscillator. By construction, for reasonable values of ξ_{int} , σ_{int} , F_{int} cannot change the deterministic steady state because it vanishes at zero and and for values much greater than ξ_{int} .

We then assume all cells interact with each other with an interaction strength that falls off with their distance. Define

$$d(C_{mn}, C_{pq}) = \sqrt{(m-p)^2 + (n-q)^2}$$
(4.12)

to be the cartesian distance between the two cells at position (m, n) and (p, q) respectively, in the array. Then they interact with an interaction strength $\tilde{\sigma}_{int} = \sigma_{int}e^{-\frac{1-d}{2}}$ such that neighbor cells for which d = 1 interact with strength S_{int} and cells separated by d > 10 interact very little.

$$M_{mn}(t) = L_t \frac{\theta_{mn}^h}{\theta_{mn}^h + t^h}$$

$$\frac{dC_{mn}[G_i]}{dt} = \alpha_i \text{Hill}(S_{mn}, T_{iM}, h_{iM}) \prod_{h_{ij} \le 0} \text{Hill}(C_{mn}[G_j], T_{ij}, h_{ij}) - \lambda_i C_{mn}[G_i]$$

$$+ C_{mn}[G_i] \sum_{p \ne m} \sum_{q \ne n} F_{int}(C_{mn}[G_i] - C_{pq}[G_i], \, \xi_{int}, \, \sigma_{int} \, e^{-\frac{d(C_{mn}, C_{pq}) - 1}{2}})$$
(4.13)

Finally, the deterministic coupled ODEs that represent these interactions are given by Eq. 4.13 where θ_{mn} is the exposure time which depends on cell position (m, n). The chemical Langevin equation is implemented as in Sec. 3.5 treating the production and degradation terms as noisy reactions. The interaction term is assumed to be exact.

4.6.2 In Silico Evolution selects for ξ_{int} , σ_{int}

The interaction parameters ξ_{int} , σ_{int} have to be carefully chosen to counteract two opposing forces. If the parameters are too small, the averaging effect will be too weak and there will be little improvement in noise robustness. If the parameters are too big, then cells which have been exposed for shorter period of time and have, therefore, achieved steady state will bias the expression of cells which are still deciding their fate.

The quotient $\frac{\sigma_{int}}{\xi_{int}}$ approximately define a timescale through which small differences in gene concentration between cells degrade to zero. If this timescale is too long, cell-to-cell interactions will not be able to mitigate the effect of noise before it decouples cells from their neighbors. If the timescale is very short, the coupling is near-instantaneous and cells will not decouple at a gene expression boundary.

To find suitable values for the interaction parameters, we run the evolution algorithm described in Sec A.1. To do so, we create a population of embryos (i.e. cell arrays equipped with the GRN) each with different parameters ξ_{int} , σ_{int} . We integrate the the embryo once deterministically without interaction terms to get $\tilde{C}_{mn}[G_i](t)$ and multiple times stochastically with the interaction term to get each time $C_{mn}[G_i](t)$. Embryos are then ranked according to their fitness (Sec. A.2) given by Eq. 4.14. Survival of the fittest dictates that embryos with bad fitness are replaced by embryos with better fitness. The population is then mutated by slightly changing ξ_{int} and σ_{int} and keeping all other parameters constant.

$$F = -\frac{1}{N_{rows}} \sum_{m} \frac{1}{N_{cols}} \sum_{n} \frac{1}{N_{genes}} \sum_{i} \sqrt{\frac{1}{N_{t}}} \sum_{t} (\tilde{C}_{mn}[G_{i}](t) - C_{mn}[G_{i}](t))^{2}$$

$$F_{avg} = \frac{1}{N_{tries}} \sum_{trials} F$$

$$(4.14)$$

For this simulation, we used N = 500, $N_{rows} = 100$, $N_{cols} = 30$, $N_{genes} = 5$, $N_t = 5000$, $N_{tries} = 5$. We set $T_{iS} = 1.59$ which gives a long timescale. The best parameters were found to be $\xi_{int} = 0.0588$ and $\sigma_{int} = 0.0300$. Figure 4–22. is the ensemble average of all cells in column 90 over 5 trials (hence the steplike properties of the graph). Comparing to Fig. 4–19 and 4–20, we conclude that cell averaging preserves the timescale and the predictive power which would otherwise be lost to noise.

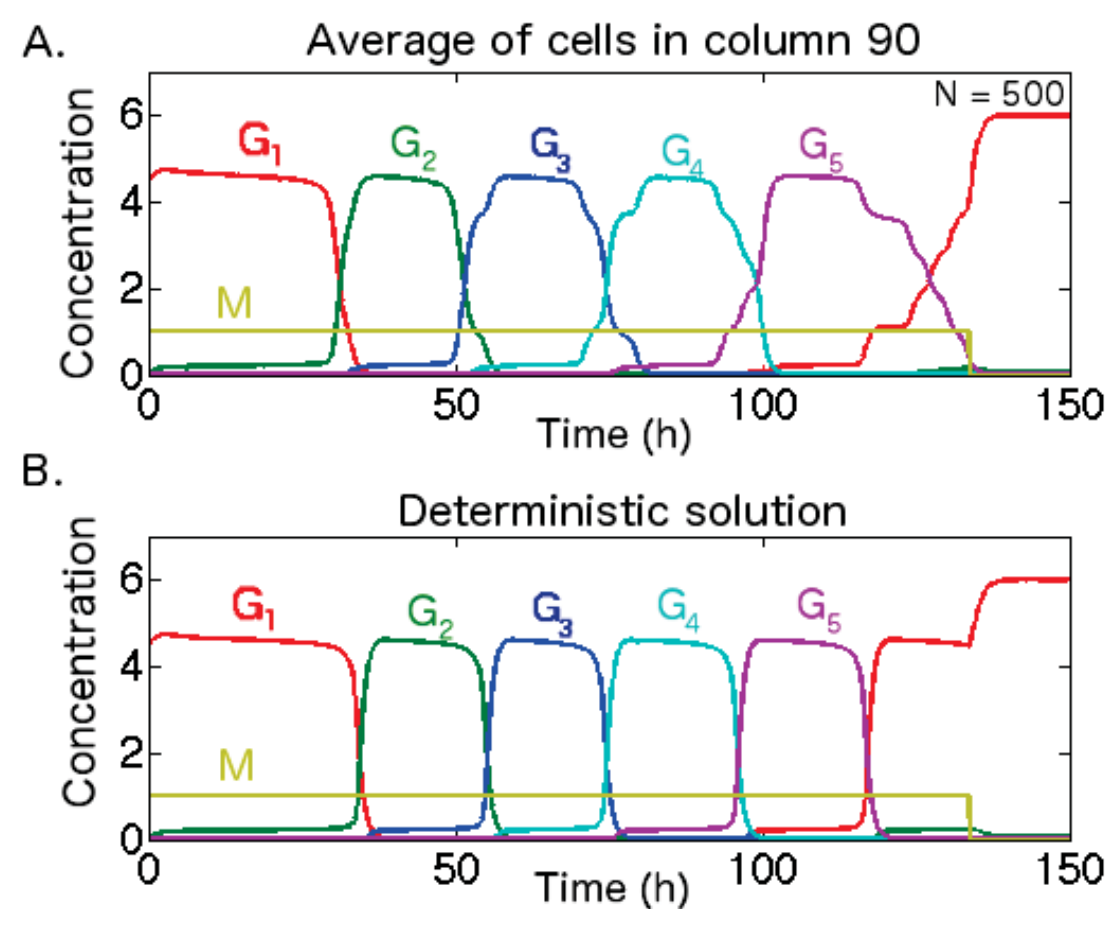


Figure 4–22: Stochastic ensemble average for N=500 with cell-to-cell interaction with $\xi=0.0588, \sigma=0.0300$ and $T_{iM}=1.59$. $M_{90}(t)$ profile is as in Fig. 4–14 with $\theta=133.8h, L_t=1$. Compare to 4–20-A. A. Average of all cells in column 90 over 5 trials. B. Deterministic, cell-autonomous solution for a cell in column 90.

Chapter 5 - Discussion

We have created a model of the embryo in Section 4.1 in which a temporal morphogenic signal is to be interpreted to generate patterning. This Temporal French Flag model necessitates a GRN which is both multistable in some regimes and incorporates a process by which cell fate is chosen based on the exposure time. The suggested GRN is highly generalizable to any number of genes, all of which are outputs. In this chapter, we discuss the implication of such a network, the experiments that can probe its behaviour and the modifications that can be done to circumvent some limitations.

5.1 Emergence of timescales and evolvability

In the Temporal French Flag model, cell fate is not only determined by a given concentration of morphogen, but also by the duration of the signal [6]. Past efforts to explain how gene networks could interpret such a signal relied on explicit timers which were added by hand. These timers are typically slowly accumulating genes which regulate other fast genes [16]. In our present work, we showed how a slow timescale can be an emerging property of a gene network. In our GRN, all degradation rates are the same and there is no special gene which acts as a timer. Instead, the network naturally follows a cascading pattern, consecutively expressing genes with a duration controlled by the proximity to a bifurcation.

The proximity to the bifurcation confers not only the slow timescale, but also a mechanism by which the gene network becomes multistable. This suggests that both timing effects and differentiation are two interconnected features of the network's dynamical properties. As others have advocated, the geometrical properties of the phase space should, therefore, play an important role in our understanding of development [40, 64, 65]. Importantly, our analysis is applicable to any number of genes and the mechanism, by virtue of bifurcation's locality, can be understood and visualized despite the large number of genes.

Interestingly, the GRN has no particular topology, all genes repress each other and it is impossible to distinguish between two genes purely from their connection (ignoring their parameters) in the directed graph. Each gene represses all the others and only the respective

parameters matter. This bolsters the idea that the richness of dynamics is more parameterdependent than topology-dependent [66]. The observed flow whereby genes are successively expressed can be generated by the nested structure of the parameters in Table 4–2 where G_i repressed weakly G_{i+1} . This structure in parameters together with the order in which genes are activated could suggest that colinearity is involved (G_i might appear sequentially in the DNA) and might imply a specific form of interactions between neighbor genes.

The inherent structure in parameter suggests an evolutionary pathway that might lead to such a gene network. A D-dimensional network can grow in size by gene duplication. Duplication of a gene and its interactions almost readily creates an extension to a D+1 version of this GRN, the only missing step is the required interaction between the last gene and the new duplicated version to replicate the pattern. To test this, we have run in silico evolutionary simulations on embryos as described in Sec. 4.4 and Fig. 4–13 with the mutual-information based fitness condition (Sec. A.2) that the resulting embryo have D domains. It is interesting to note that while we did not specifically select for it, the resulting networks did exhibit the ability to alter the timescale. However, the mechanism was never as clean as the one presented in Sec. 4.5 due to the more complex interaction between the many genes. Details are given appendix B.

5.2 Gene knocking and comparison to previous models

There are two types of gene knocking experiments that can be done directly on our model. The first one is complete removal of a gene. The easiest way to knock out gene G_i is to set the production rate $\alpha_i = 0$, this insures that the gene will never be expressed spontaneously. It is easy to see that removing G_i in our model simply amounts to removing the bridge between G_{i-1} and G_{i+1} . The only gene which can be expressed concurrently with G_{i-1} is G_i , and the only way G_{i+1} can ever take off is if G_i is expressed. The end result is a system which can never proceed to the later fates of G_{i+1}, G_{i+2}, \ldots It is effectively by prohibiting imposing strong repression that we prohibit the transition $G_5 \to G_1$. Without this repression the system behaves like an oscillator.

The second way we can knock off a gene is to do it temporarily by exposing the cell to a strong repressor. This doesn't change $\alpha_i \neq 0$ and it allows the system to keep producing G_i .

By adding a strong repressor, we can temporarily suppress $G_i \to 0$. We model this as setting $G_i = 0$ at some time t and letting the system continue its time course as if nothing happened. Doing this to our GRN, the genes G_{i+1}, G_{i+2}, \ldots are progressively expressed with increasing amplitude and a short period, until the system stabilizes in the last state or retraces its oscillating cycle (when $G_D \to G_1$ is allowed). The timescale is greatly affected as can be seen in Fig. 5–1.

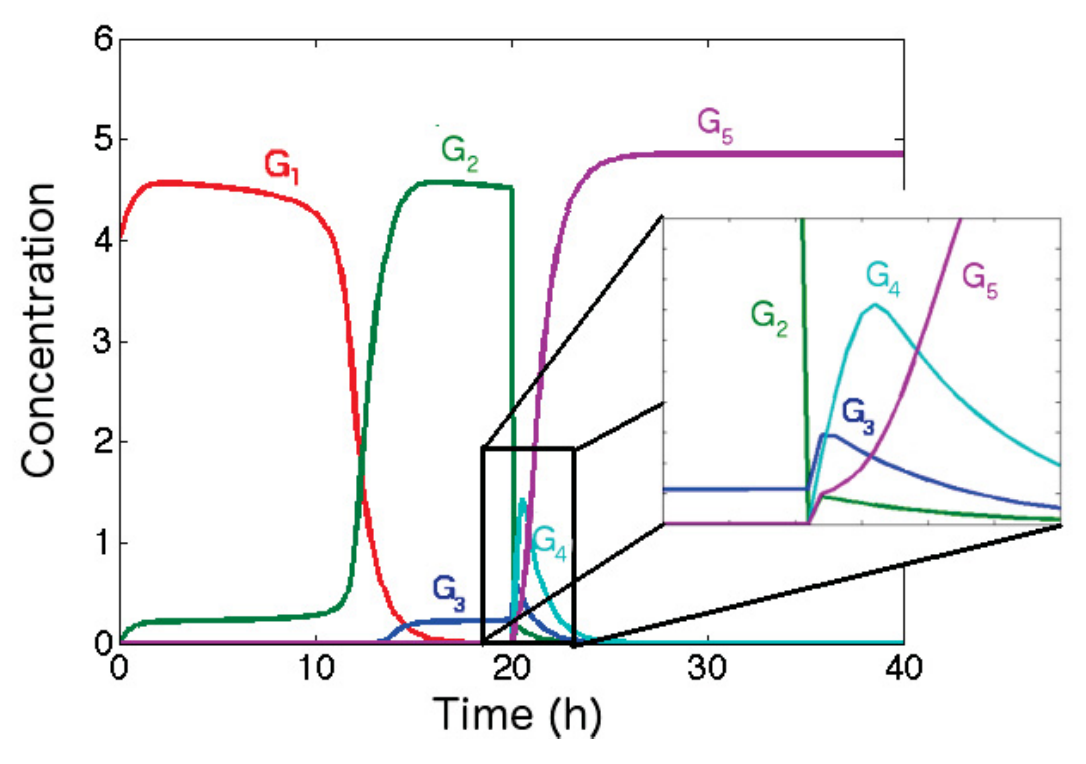


Figure 5–1: Temporary gene knock off in the 5D GRN. We set $G_3=0$ at t=20. The system continues in the same order $G_3\to G_4\to G_5$ but with increasing amplitude and a fast timescale.

The previous models of Francois [16], which used an explicit timer, do not react in the same way to such a gene knock out. Instead, after G_i is set to zero, the system re-expresses G_i and resumes its normal time course. This is because the genes are slaved to the slow time gene. Their expression is directly tied to the expression of the timer gene in a way such that setting $G_i = 0$ merely delays the system shortly as G_i rises back to its previous levels. This provides a method by which experiment can distinguish between a model with an emerging timescale and one with an explicit timer.

Although, the model in this form is not robust to removal of genes, it is theoretically possible to duplicate the network and add some interactions between the duplicated network to create a redundancy which makes the network resistant to gene deletion. Imagine an oscillating GRN in which $G_D \to G_1$ is allowed. The two networks of genes G_i and the duplicated F_i act like two coupled oscillators in the high morphogen regime. As time progresses, G_i transitions to G_{i+1} and then to G_{i+2} and so on. In the absence of G_{i+1} , the interactions due to F_{i+1} allows G_{i+2} to rise and keep the oscillation going. The Hox clusters might be such a type of network duplication and it is known that deletion of certain Hox genes leads to the formation of anterior structures [19, 22].

This type of modification comes at a cost however. The redundancy introduced leads to a doubling in the size of the gene network as many regulator genes have to be added. The timescale is also not controlled by the bifurcation anymore as the duplicated network controls the activation of the successive gene. It is not clear whether this trade-off is necessary and it might not be possible to keep both the bifurcation and the robustness to gene deletion.

5.3 Future directions

There models presented in this work raise many questions. Although we have implemented a cell-to-cell interaction scheme to provide noise robustness, the effect of noise in dynamical based systems is still a relevant issue to be explored. Is the sensibility to a critical parameter, like T_{iM} in direct contradiction with the prevailing stochastic nature of biological systems? Is a static morphogen gradient a better mechanism for patterning in a noisy environment [56]?

Finally, criticality¹ has been invoked in many biological processes [67,68]. In fly development, the gap genes mutually repress each other and the dynamical flow has been observed to be canalized [69]. The underlying mechanism that leads to this canalization still remains largely unknown, however, our model predicts canalization as a result of the slow manifold and the two problems might be more similar than they look. On the other hand,

¹ Criticality is hard to define, especially in this context, and refers to a vast array of phenomena. In our case, it is the transition to an infinite timescale during a saddle-node bifurcation.

it has been found that the gap genes exhibit strong correlations at their boundary [67]. It is argued that the boundary between gap genes is a byproduct of criticality and our model similarly predicts strong correlations in-between peaks of the valley due to canalization. The relationship between these two types of criticality is still unclear, in our case it happens under a dynamical morphogen while in the fly, it is under the control of steady morphogen gradients. The two might be closely related and we suggest that an in-depth analysis of the correlations $\langle G_i, G_j \rangle$ as a function of time might reveal similarities.

Appendix A - Computational Evolution

There is something very appealing about simulating the process of evolution. It is a clever process which through selection overcomes the odds and allows the needle to be separated from the hay. However, what nature does, we have yet to reproduce but in a crude way. We can select through a fitness function, for a specific pattern formation, but the result can often be disappointing. There are often fringe cases which can satisfy a given fitness function, yet only through a loophole we overlooked. There is the danger of fine-tuning, a network might be selected for with great agreement with the fitness function, but depend too heavily on unimportant parameters. Generating a network in agreement with broad and flexible principles is sometimes as much of an art as it is a science.

We give here the outlines of Francois' evolution algorithm [16,70] through which we can select for network topology, parameters or test models according to a fitness function. It is a great resource for the biologist who wishes to test models with networks in a systematic way. Francois' algorithm has been able to produce working networks whose complexity might have prohibited a more pedestrian approach.

A.1 Evolution Algorithm

The evolution algorithm tries to mimic nature as closely as possible. We break the process into conceptual steps.

- The evolution algorithm selects at the generation level
- Each generation corresponds to a population of networks
- The population is made up of a number of organisms networks, each represented as a network with its own topology and parameters
- The organism develops in silico. We construct an array of cells governed by the organism's network, an input morphogen and the underlying model which can include things such as cell to cell interactions, or artificial gene inhibition mid-development.
- The array of cell is integrated (perhaps multiple times, perhaps with noise) and the resulting output for each cell is issued. Output can be genes' concentration at steady-state or even the entire time series.

- The output is used to evaluate the fitness for each organism. It is up to the biologist to carefully select a fitness function according to his needs.
- The population is ranked according to their fitness (smaller fitness is better) and individuals with poor fitness are discarded.
- Fit individuals are allowed to mutate and take part in the next generation. Mutations are random, sparse and can either change the topology or parameters of a certain interaction.

Some shortfalls of the algorithm include speed and scalability. Convergence to a fit network can be very slow. In addition, the bigger the networks the longer the selection process takes. Big networks tend to have many more parameters and therefore a much greater parameter-space has to be explored. It is possible to speed up the process by sequentially evolving bigger networks. A three gene network might converge relatively quickly. One can then duplicate an existing gene to generate a four gene network. Because the network is based on an already working three dimensional network, convergence with four genes might happen much faster. The process can then be repeated until sufficiently big networks have been generated.

A.2 Fitness Function

The fitness function is the core of the evolution algorithm. Without it, the algorithm is nothing more than a brute force attack on the parameter space. In order to avoid bad surprises, it is imperative to choose a fitness function that is well understood. We give here two examples relevant to the present work.

The first fitness function serves to select for patterns along a cell array of length L. We look for a fitness which creates a clear distinction between domains, so that better fitness is acheived if a single output gene is expressed. We also look for even domains, so that each domain has similar length. Suppose C_{im} is the concentration of the realization gene i in cell m, then a good candidate fitness is mutual information [71] given by Eq. A.1. By maximizing the mutual information between genes across the array of cells, we create domains where only one gene can be activated and embryos where all genes are represented equally. The mutual information is then a negative scalar (more negative is better) on the

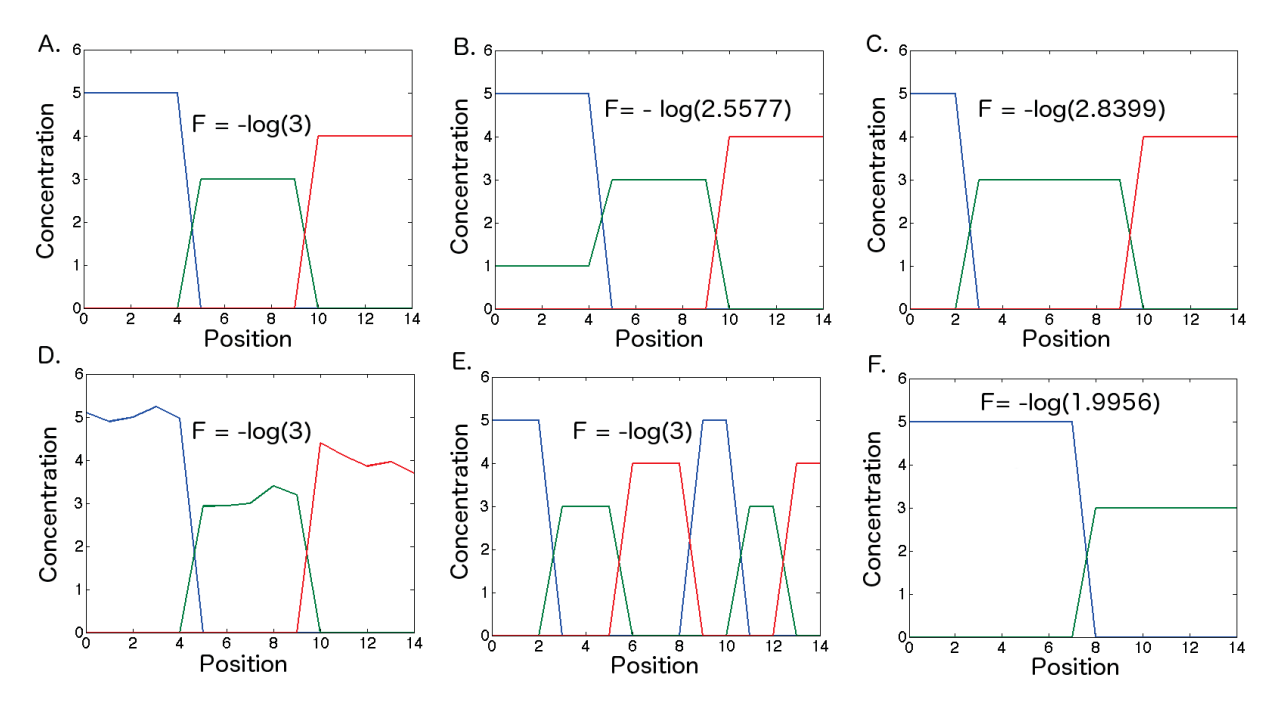


Figure A–1: Mutual Information of various cell arrays. A. N perfect equal domains has perfect fitness $F = -\log(N)$ so that three domains have fitness $F = -\log(3)$. B. Overlap between domains is penalized, $F = -\log(2.5577)$ C. Uneven domains are penalized. $F = -\log(2.8399)$. D. As long as there is no domain overlap, noise does not change the fitness, $F = -\log(3)$. E. The domains do not have to be continuous, $F = -\log(3)$. F. Two almost even domains lead to near perfect fitness $F = -\log(1.9956)$

order of -ln(N) where N is the number of domains. Fig. A–1 shows the fitness of various cell arrays. Three equal and clear domains lead to perfect fitness. Overlaps between domains is penalized, and so are domains that are too short or too long. As long as the domains do not overlap, the actual value of the realizator gene does not matter and neither does the continuity of the domains. As a consequence, if we want only two consecutive domains, this fitness function is not enough. If the clustering of domains matters, it is then necessary to add another term to our fitness function, perhaps one that counts the number of boundaries between domains and tries to minimize it.

$$F = \sum_{i} p_{i} \log(p_{i}) + \sum_{m} p_{m} \log(p_{m}) - \sum_{i} \sum_{m} p_{im} \log(p_{im})$$
Where $p_{im} = \frac{C_{im}}{L \sum_{k} C_{km}}$, $p_{i} = \sum_{m} p_{im}$ and $p_{m} = \frac{1}{L}$. (A.1)

The second fitness function we present is meant to select for noise robustness. An array of cells could be computed in two ways, one by integrating the network in a cell autonomous way and the other by allowing cell-to-cell interactions. If we wish to test our mechanism for cell-to-cell interaction as a means of noise reduction, we might conjure a fitness which compares the deterministic time series to the stochastic time series. By integrating both for each cell, we can compare them through the quadratic mean of their difference. Suppose $\vec{x}(t_i)$ is the time series for the deterministic run and $\vec{x}(t_i)$ that of the stochastic time series. Eq. A.2 counts the deviation from the deterministic time series where n is the number of time steps.

$$F(\vec{x}(t), \vec{\tilde{x}}(t)) = \frac{1}{N_{genes}} \sum_{j} \sqrt{\sum_{t_i} \frac{(x_j(t_i) - \tilde{x}_j(t_i))^2}{n}}$$
(A.2)

When F is at a minimum, the two time series are identical. In practice, x and \tilde{x} will never be identical, but if we manage to select a good model and good parameters, we can hope to minimize the effect the effect of noise on \tilde{x} . Fig. A–2 shows the fitness of three Langevin realization of the biological switch, Eq. 3.7, which we introduced in Sec. 3.4. As expected the fitness function decreases as N, the number of molecules per volume which quantifies the noise level, increases.

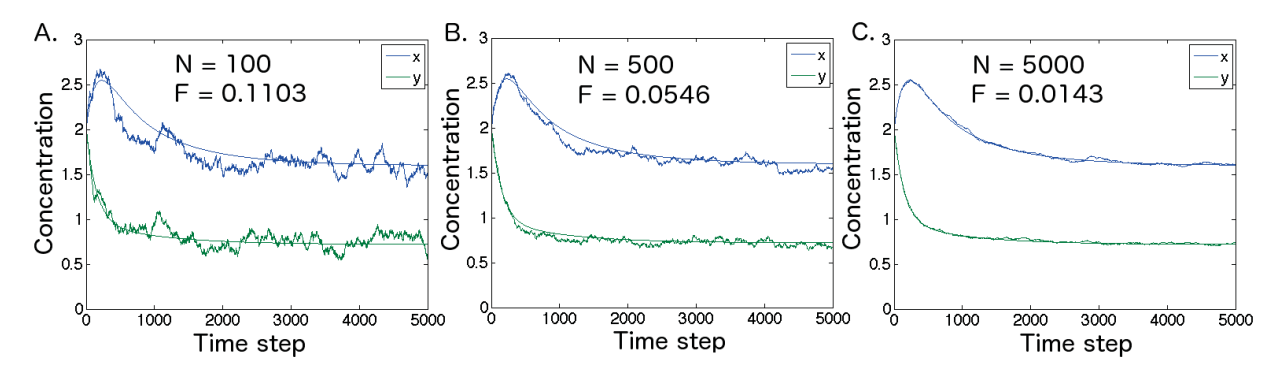


Figure A–2: RMS fitness for three different Langevin realizations of the noise for the biological switch, Eq. 3.7 with a = 0.45, b = 1. A. N = 100 leads to a fitness of F = 0.1103. B. N = 500 has fitness F = 0.0546. C. N = 5000 is nearly deterministic with F = 0.0143.

Appendix B - Evolution of temporal networks

To model developmental patterning under the influence of a temporal morphogen signal, we have used the evolutionary algorithm described in Appendix A. We have selected for multidimensional networks which give rise to domains according to the setup of Fig. 4–13. That is, we model M(t) as a traveling wave along the embryo which stabilizes after θ_m time in cell m corresponding to the exposure time. We have assumed a fully repressing network where all genes repress each other, we have further assumed that M represses all genes.

Eq. B.1 is the set of coupled ODEs for each cell C_m in the array. $C_m[G_i]$ is the concentration of gene G_i in cell m. Once the equations have been integrated deterministically, an array C_{im} is filled with the concentration of genes i at cell m. The fitness is then computed from C_{im} using mutual information (Eq. A.1). The best network is selected according to the most negative fitness and each generation new mutations are introduced. We fix the topology of the network and choose to mutate the Hill coefficients and thresholds of random nodes.

$$M_m(t) = L_t \frac{\theta_m^{\eta}}{\theta_m^{\eta} + t^{\eta}}$$

$$\dot{C}_m[G_i] = \alpha_i \text{Hill}(M_m(t), T_{iM}, h_{iM}) \prod_{h_{ij} \leq 0} \text{Hill}(C_m[G_j], T_{ij}, h_{ij}) - \lambda_i C_m[G_i]$$
(B.1)

Given the enormous parameter space for a higher dimensional GRN, evolving an maximum number of domains is an ardous task. To speed up the process we evolved the network in increasing dimensions. First, we evolved a 3D network first which can give three domains. We then duplicated the last gene to get a 4D network which will give three domains. We let the evolution algorithm select for parameters so that the 4D network can give four domains. Once we have four domains, we duplicate the last gene again and select for parameters that allow for five domains. The resulting network parameters are given in Table B–1. The interactions are very entangled due to the random nature of mutations. In some cases, it is possible to see how some parameters were left unchanged after duplication.

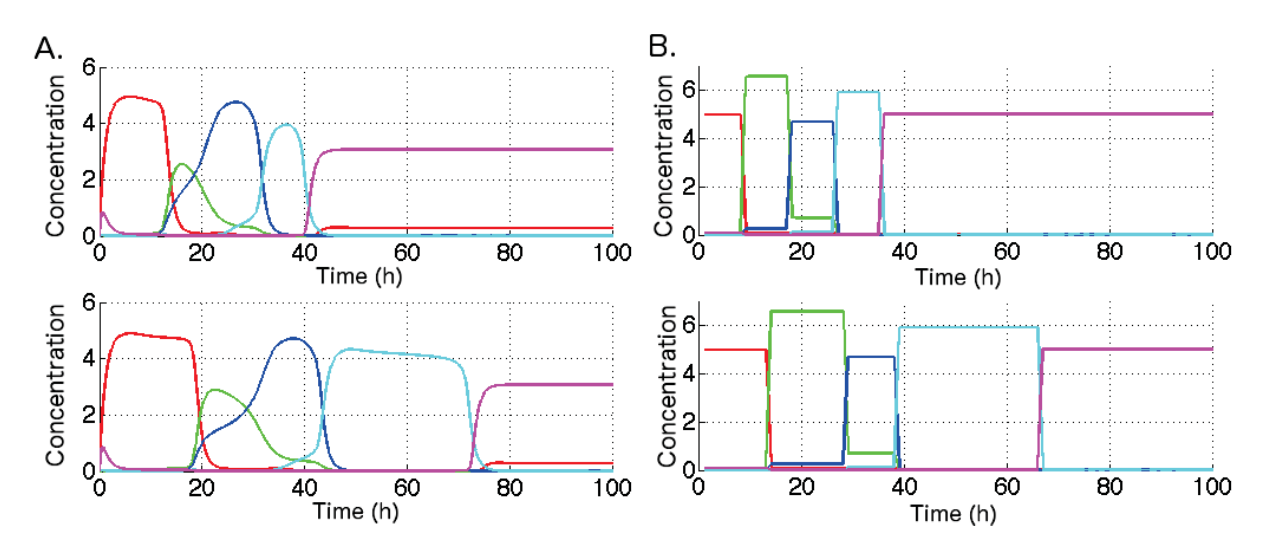


Figure B–1: Time course (A) and gene expression domains (B) for an evolved GRN. Gene activation is sequential and it is possible to control the timescale by changing T_{iM} . However, the interactions between genes tend to be such that the timescales are entangled and cannot be entirely isolated for a single gene.

Top: $T_{1M} = 4.59$, $T_{2M} = 0.987$, $T_{3M} = 2.64$, $T_{4M} = 1.53$, $T_{5M} = 2.48$, Bottom: $T_{1M} = 3.30$, $T_{2M} = 1.10$, $T_{3M} = 2.30$, $T_{4M} = 1.82$, $T_{5M} = 2.48$.

Nevertheless, the GRN still leads to patterning when exposed to a temporal morphogen gradient. Fig. B–1 shows the time course and the associated domains for two sets of thresholds T_{iM} . Interestingly, there is a change of timescale and domain length when changing T_{iM} . Mutual information select for domains of equal size, but it does not select for the network's ability to alter the domain's length. This result implies that networks based on temporal signaling are likely to be those equipped with the ability to adapt to the timescale provided by the morphogen.

Rates						
	G_1	G_2	G_3	G_4	G_5	
Production α	5	5	5	5	5	
Degradation γ	1	0.761	1	0.847	1	

	Hill Coefficients h_{ij} and T_{iM}						
	G_1	G_2	G_3	G_4	G_5	M	
G_1	0	2.2	1.58	3.62	4.14	3.43	
G_2	4.38	0	3.05	4.73	4.14	1.36	
G_3	1.42	2.70	0	3.57	4.14	4.72	
G_4	2.31	3.65	4.00	0	4.14	1.75	
G_5	3.64	0.847	4.84	4.80	0	0.515	

Treshholds T_{ij} and T_{iM}						
	G_1	G_2	G_3	G_4	G_5	M
G_1	0	1.21	0.431	0.226	1.57	4.59
G_2	4.06	0	2.35	0.699	0.0325	0.987
G_3	1.39	2.22	0	0.950	0.0325	2.64
G_4	1.38	0.0336	3.71	0	0.325	1.53
G_5	1.70	1.32	0.0840	1.40	0	2.48

Table B–1: Table for the n=5 dimensional evolved GRN.

References

- [1] L Wolpert. Evolution of the cell theory. *Philosophical Transactions of the Royal Society of London. Series B: Biological Sciences*, 349(1329):227–233, 1995.
- [2] Klaus Sander. Landmarks in developmental biology (5) 'mosaic work' and 'assimilating effects' in embryogenesis: Wilhelm roux's conclusions after disabling frog blastomeres. Development Genes and Evolution, 200(5):237–239, 1991.
- [3] Klaus Sander. Shaking a concept: Hans driesch and the varied fates of sea urchin blastomeres. *Development Genes and Evolution*, 201(5):265–265, 1992.
- [4] Richard Harland and John Gerhart. Formation and function of spemann's organizer. Annual review of cell and developmental biology, 13(1):611–667, 1997.
- [5] Martin Hrabé de Angelis, Heinrich Flaswinkel, Helmut Fuchs, Birgit Rathkolb, Dian Soewarto, Susan Marschall, Stephan Heffner, Walter Pargent, Kurt Wuensch, Martin Jung, et al. Genome-wide, large-scale production of mutant mice by enu mutagenesis. *Nature genetics*, 25(4):444–447, 2000.
- [6] Lewis Wolpert. Principles of Development. Oxford University Press, 2006.
- [7] Lewis Wolpert. Positional information and the spatial pattern of cellular differentiation. Journal of theoretical biology, 25(1):1–47, 1969.
- [8] Christopher H Contag and Michael H Bachmann. Advances in in vivo bioluminescence imaging of gene expression. *Annual Review of Biomedical Engineering*, 4(1):235–260, 2002.
- [9] Steven G Kuntz and Michael B Eisen. Native climate uniformly influences temperature-dependent growth rate in Drosophila embryos. arXiv.org, June 2013.
- [10] Alexander Aulehla and Olivier Pourquié. Signaling Gradients during Paraxial Mesoderm Development. Cold Spring Harbor Perspectives in Biology, 2(2):1–17, February 2010.
- [11] Olivier Pourquié. The segmentation clock: converting embryonic time into spatial pattern. *Science*, 301(5631):328–330, 2003.
- [12] C E Nelson, B A Morgan, A C Burke, E Laufer, E DiMambro, L C Murtaugh, E Gonzales, L Tessarollo, L F Parada, and Clifford J Tabin. Analysis of Hox gene expression in the chick limb bud. *Development (Cambridge, England)*, 122(5):1449–1466, May 1996.
- [13] Brian D Harfe, Paul J Scherz, Sahar Nissim, Hua Tian, Andrew P McMahon, and Clifford J Tabin. Evidence for an expansion-based temporal Shh gradient in specifying vertebrate digit identities. *Cell*, 118(4):517–528, August 2004.
- [14] Nikolaos Balaskas, Ana Ribeiro, Jasmina Panovska, Eric Dessaud, Noriaki Sasai, Karen M. Page, James Briscoe, and Vanessa Ribes. Gene Regulatory Logic for Reading the Sonic Hedgehog Signaling Gradient in the Vertebrate Neural Tube. Cell, 148(1-2):273–284, 2012.

- [15] Hans Meinhardt. Models of biological pattern formation. Academic Pr, 1982.
- [16] Paul François and Eric Dean Siggia. Predicting embryonic patterning using mutual entropy fitness and in silico evolution. *Development (Cambridge, England)*, 137(14):2385–2395, June 2010.
- [17] Jasmina Panovska-Griffiths, Karen M. Page, and James Briscoe. A gene regulatory motif that generates oscillatory or multiway switch outputs. *Journal of the Royal Society*, *Interface / the Royal Society*, 10(79):20120826, February 2013.
- [18] Gines Morata. Homeotic genes of *Drosophila*. Current opinion in genetics & development, 3(4):606–614, 1993.
- [19] Edward B Lewis et al. A gene complex controlling segmentation in drosophila. *Nature*, 276(5688):565–570, 1978.
- [20] Frank H Ruddle, Janet L Bartels, Kevin L Bentley, Claudia Kappen, Michael T Murtha, and John W Pendleton. Evolution of hox genes. Annual review of genetics, 28(1):423– 442, 1994.
- [21] Derek Lemons and William McGinnis. Genomic evolution of hox gene clusters. *Science*, 313(5795):1918–1922, 2006.
- [22] Eric van Den Akker, Catherine Fromental-Ramain, Wim de Graaff, Hervé Le Mouellic, Philippe Brûlet, Pierre Chambon, and Jacqueline Deschamps. Axial skeletal patterning in mice lacking all paralogous group 8 hox genes. *Development*, 128(10):1911–1921, 2001.
- [23] C Tickle. Patterning systems —from one end of the limb to the other. *Developmental* cell, 4(4):449–458, 2003.
- [24] Jean-Denis Bénazet and Rolf Zeller. Vertebrate limb development: moving from classical morphogen gradients to an integrated 4-dimensional patterning system. *Cold Spring Harbor perspectives in biology*, 1(4):a001339, 2009.
- [25] C Tickle. The number of polarizing region cells required to specify additional digits in the developing chick wing. 1981.
- [26] Dennis Summerbell. A quantitative analysis of the effect of excision of the aer from the chick limb-bud. *Journal of embryology and experimental morphology*, 32(3):651–660, 1974.
- [27] Lee Niswander, Cheryll Tickle, Astrid Vogel, Iain Booth, and Gail R Martin. Fgf-4 replaces the apical ectodermal ridge and directs outgrowth and patterning of the limb. *Cell*, 75(3):579–587, 1993.
- [28] Robert D Riddle, Randy L Johnson, Ed Laufer, and Cliff Tabin. Sonic hedgehog mediates the polarizing activity of the zpa. *Cell*, 75(7):1401–1416, 1993.
- [29] L Wolpert, C Tickle, M Sampford, and JH Lewis. The effect of cell killing by x-irradiation on pattern formation in the chick limb. *Journal of embryology and experimental morphology*, 50(1):175–198, 1979.

- [30] Eric Dessaud, Lin Lin Yang, Katy Hill, Barny Cox, Fausto Ulloa, Ana Ribeiro, Anita Mynett, Bennett G Novitch, and James Briscoe. Interpretation of the sonic hedgehog morphogen gradient by a temporal adaptation mechanism. *Nature*, 450(7170):717–720, 2007.
- [31] Eric Dessaud, Vanessa Ribes, Nikolaos Balaskas, Lin Lin Yang, Alessandra Pierani, Anna Kicheva, Bennett G Novitch, James Briscoe, and Noriaki Sasai. Dynamic assignment and maintenance of positional identity in the ventral neural tube by the morphogen sonic hedgehog. *PLoS biology*, 8(6):e1000382, 2010.
- [32] Thomas M Jessell. Neuronal specification in the spinal cord: inductive signals and transcriptional codes. *Nature Reviews Genetics*, 1(1):20–29, 2000.
- [33] J Ericson, P Rashbass, A Schedl, SKAWAKAMI Brenner-Morton, A Kawakami, V Van Heyningen, TM Jessell, and J Briscoe. Pax6 controls progenitor cell identity and neuronal fate in response to graded shh signaling. *Cell*, 90(1):169–180, 1997.
- [34] J Briscoe, L Sussel, P Serup, D Hartigan-O'Connor, TM Jessell, JLR Rubenstein, and J Ericson. Homeobox gene nkx2. 2 and specification of neuronal identity by graded sonic hedgehog signalling. *Nature*, 398(6728):622–627, 1999.
- [35] Bennett G Novitch, Albert I Chen, and Thomas M Jessell. Coordinate regulation of motor neuron subtype identity and pan-neuronal properties by the bhlh repressor olig2. *Neuron*, 31(5):773–789, 2001.
- [36] Nigel Goldenfeld. Lectures on phase transitions and the renormalization group. 1992.
- [37] J Hopfield. Neural networks and physical systems with emergent collective computational abilities. *Proceedings of the National Academy of Sciences*, 79(8):2554–2558, 1982.
- [38] Fa-Yueh Wu. The potts model. Reviews of modern physics, 54(1):235, 1982.
- [39] Hidde De Jong. Modeling and simulation of genetic regulatory systems: a literature review. *Journal of computational biology*, 9(1):67–103, 2002.
- [40] Johannes Jaeger, David Irons, and Nick Monk. The Inheritance of Process: A Dynamical Systems Approachs. *Journal of Experimental Zoology Part B: Molecular and Developmental Evolution*, pages 1–22, October 2012.
- [41] James N Weiss. The hill equation revisited: uses and misuses. *The FASEB Journal*, 11(11):835–841, 1997.
- [42] Gašper Tkačik, Curtis G Callan, and William Bialek. Information flow and optimization in transcriptional regulation. *Proceedings of the National Academy of Sciences*, 105(34):12265–12270, 2008.
- [43] Steven H Strogatz. Nonlinear dynamics and chaos (with applications to physics, biology, chemistry a. Perseus Publishing, 2006.
- [44] Louis N Hand and Janet D Finch. *Analytical mechanics*, volume 18. Cambridge University Press Cambridge, 1998.

- [45] Jack Carr. Applications of centre manifold theory. Springer, 1979.
- [46] B Hassard and Y.H Wan. Bifurcation formulae derived from center manifold theory. Journal of Mathematical Analysis and Applications, 63(1):297 – 312, 1978.
- [47] AJ Roberts. The application of centre-manifold theory to the evolution of system which vary slowly in space. The Journal of the Australian Mathematical Society. Series B. Applied Mathematics, 29(04):480–500, 1988.
- [48] George WA Constable, Alan J McKane, and Tim Rogers. Stochastic dynamics on slow manifolds. *Journal of Physics A: Mathematical and Theoretical*, 46(29):295002, 2013.
- [49] Petra Boxler. A stochastic version of center manifold theory. *Probability Theory and Related Fields*, 83(4):509–545, 1989.
- [50] J L Cherry and F R Adler. How to make a biological switch. *Journal of Theoretical Biology*, 203(2):117–133, March 2000.
- [51] Richard Losick and Claude Desplan. Stochasticity and cell fate. *Science*, 320(5872):65–68, 2008.
- [52] Hana El Samad, Mustafa Khammash, Linda Petzold, and Dan Gillespie. Stochastic modelling of gene regulatory networks. *International Journal of Robust and Nonlinear Control*, 15(15):691–711, 2005.
- [53] Brian Munsky, Gregor Neuert, and Alexander van Oudenaarden. Using gene expression noise to understand gene regulation. *Science*, 336(6078):183–187, 2012.
- [54] Thomas R. Sokolowski, Thorsten Erdmann, and Pieter Rein ten Wolde. Mutual repression enhances the steepness and precision of gene expression boundaries. *PLoS Comput Biol*, 8(8):e1002654, 08 2012.
- [55] Kirsten H ten Tusscher and Paulien Hogeweg. Evolution of Networks for Body Plan Patterning; Interplay of Modularity, Robustness and Evolvability. *PLoS Comput Biol*, 7(10):e1002208, October 2011.
- [56] Thomas Gregor, David W. Tank, Eric F. Wieschaus, and William Bialek. Probing the limits to positional information. *Cell*, 130(1):153 164, 2007.
- [57] Ga šper Tkačik, Curtis G. Callan, and William Bialek. Information capacity of genetic regulatory elements. *Phys. Rev. E*, 78:011910, Jul 2008.
- [58] Nicolaas Godfried Van Kampen. Stochastic processes in physics and chemistry, volume 1. Elsevier, 1992.
- [59] Daniel T Gillespie. A general method for numerically simulating the stochastic time evolution of coupled chemical reactions. *Journal of Computational Physics*, 22(4):403 434, 1976.
- [60] Daniel T Gillespie. Stochastic simulation of chemical kinetics. *Annual review of physical chemistry*, 2007.

- [61] Wei W Sha, Jonathan J Moore, Katherine K Chen, Antonio D AD Lassaletta, Chung-Seon CS Yi, John J JJ Tyson, and Jill C JC Sible. Hysteresis drives cell-cycle transitions in Xenopus laevis egg extracts. *Proceedings of the National Academy of Sciences of the United States of America*, 100(3):975–980, February 2003.
- [62] Fengzhu Xiong, Andrea R Tentner, Peng Huang, Arnaud Gelas, Kishore R Mosaliganti, Lydie Souhait, Nicolas Rannou, Ian A Swinburne, Nikolaus D Obholzer, Paul D Cowgill, Alexander F Schier, and Sean G Megason. Specified neural progenitors sort to form sharp domains after noisy shh signaling. Cell, 153(3):550–561, April 2013.
- [63] Annette L Parks, Kristin M Klueg, Jane R Stout, and MA Muskavitch. Ligand endocytosis drives receptor dissociation and activation in the notch pathway. *Development*, 127(7):1373–1385, 2000.
- [64] Paul François and Eric Dean Siggia. Phenotypic models of evolution and development: geometry as destiny. Current Opinion in Genetics & Development, pages –, September 2012.
- [65] Francis Corson and Eric Dean Siggia. Geometry, epistasis, and developmental patterning. *Proc Natl Acad Sci U S A*, 109(15):5568–5575, April 2012.
- [66] M Tikhonov and William Bialek. [1308.0317] Complexity in genetic networks: topology vs. strength of interactions. arXiv.org, 2013.
- [67] D Krotov, Julien O Dubuis, Thomas Gregor, and William Bialek. Morphogenesis at criticality?
- [68] Thierry Mora and William Bialek. Are Biological Systems Poised at Criticality? *Journal of Statistical Physics*, 144(2):268–302, July 2011.
- [69] Manu, Svetlana Surkova, Alexander V Spirov, Vitaly V Gursky, Hilde Janssens, Ah-Ram Kim, Ovidiu Radulescu, Carlos E Vanario-Alonso, David H Sharp, Maria Samsonova, and John Reinitz. Canalization of gene expression and domain shifts in the Drosophila blastoderm by dynamical attractors. *PLoS Comput Biol*, 5(3):e1000303, March 2009.
- [70] Paul François. Evolution in silico: From network structure to bifurcation theory. In *Evolutionary Systems Biology*, pages 157–182. Springer, 2012.
- [71] Thomas M Cover and Joy A Thomas. *Elements of information theory*. John Wiley & Sons, 2012.